UNIVERSITY OF CALIFORNIA
RIVERSIDE

A Study of Photoproduction of Vector Mesons on Deuterium by 5.5 GeV Linearly Polarized Photons

A Dissertation submitted in partial satisfaction
of the requirements for the degree of

Doctor of Philosophy

in

Physics

by

Virendra Prakash Gupta

December, 1974

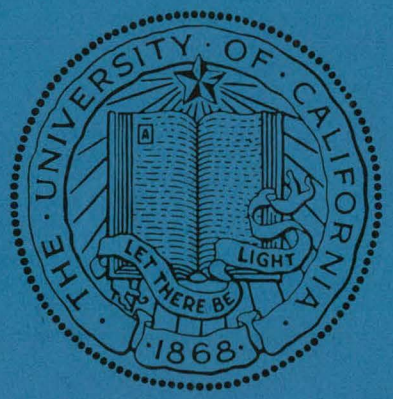

DISCLAIMER

MASTER

UNIVERSITY OF CALIFORNIA
RIVERSIDE

A Study of Photoproduction of Vector Mesons on Deuterium by 5.5 GeV Linearly Polarized Photons

A Dissertation submitted in partial satisfaction
of the requirements for the degree of

Doctor of Philosophy

in

Physics

by

Virendra Prakash Gupta

December, 1974

Disscrtation Committee:

Professor Sun-Yiu Fung, Chairman

Professor Anne Kernan

Professor Robert T. Poe

The dissertation of Virendra Prakash Gupta is approved:

Anne Kerman

Robert T. Pol

Sun-Yin Tung
Committee Chairman

University of California, Riverside

December, 1974

ACKNOWLEDGEMENTS

I wish to thank Professor Sun-Yiu Fung, my thesis advisor, for his encouragement and guidance for the successful completion of this work. I will always remember his friendly and receptive manner.

I am indebted to Professors Robert T. Poe, Benjamin C. Shen, and Anne Kernan for the help and fruitful discussions I have had with them from time to time.

I also wish to thank the members of Ely Group at LBL, especially, Dr. George Gidal for the assistance he has given me. I express my sincere appreciation to all the people from Riverside and LBL who have helped me during the course of this work. I am particularly grateful to Dr. Terry Schalk (presently at SLAC) and Mr. William Marsh with whom I have had many interesting discussions.

I am thankful to the scanners of Riverside and LBL, and the measuring personnel of LBL for their diligent work. The help and cooperation of the SLAC crew for performing this experiment is gratefully acknowledged.

Finally, I would like to thank my wife Shakuntala for her patience, understanding, and support during the last five years.

This work was done under the auspices of the Atomic Energy Commission.

To

My Grandparents

ABSTRACT OF THE DISSERTATION

A Study of Photoproduction of Vector Mesons on Deuterium by 5.5 GeV Linearly Polarized Photons

by

Virendra Prakash Gupta

Doctor of Philosophy, Graduate Program in Physics
University of California, Riverside, December 1974
Professor Sun-Yiu Fung, Chairman

We present here the experimental results of a deuterium bubble chamber photoproduction study of half a million pictures at 5.5 GeV. This experiment has been performed using a monoenergetic and linearly polarized photon beam facility at SLAC. At 5.5 GeV the beam polarization is greater than 90%, and the average FWHM of the beam energy spectrum is 0.6 GeV.

The reaction $\gamma d \rightarrow \pi^+\pi^- d$ has been studied in detail. We obtained a clear sample of $\gamma d \rightarrow \rho^o d$ channel and using the ρ^o decay distribution in terms of an extended density matrix which includes correlation with the beam polarization, we have been able to determine nine independent density matrix

parameters.

The study of ρ^o production and decay in the reaction channel $\gamma d \rightarrow \rho^o d$ was found to proceed almost completely through natural parity exchanges; the contribution from unnatural parity exchanges being only (5.3 ± 4.5)% for momentum transfer $|t| \lesssim 0.25$ GeV^2. It has been observed that the ρ^o production mechanism conserves s-channel c.m.s. helicity for $|t| \lesssim 0.15$ GeV^2.

After carrying out the fitting to the $\pi^+\pi^-$ mass distribution, we obtained for the ρ^o mass and width the values (766 ± 5) and (139 ± 11) MeV, respectively. The ρ^o production cross section in this channel has been determined to be (9.1 ± 0.8) μb.

We have also looked into the final states $\pi^+\pi^-\pi^o d$, $K^+K^- d$, $\pi^+\pi^+\pi^-\pi^- d$, and $\pi^+\pi^-\pi^- pp$ for the production of ω, ϕ, ρ', and A_1 mesons, respectively. However, due to insufficient statistics, no conclusive remarks could be made.

TABLE OF CONTENTS

LIST OF TABLES

LIST OF FIGURES

I. INTRODUCTION

Photon induced reactions have played an important role in the field of nuclear and elementary particle physics in the last thirty years. Evidences for the existence of many particles and resonances first came from photoproduction experiments. In 1948 charged pions, whose existence had been proven previously only through cosmic-ray events, were photo-produced in the laboratory. Neutral pi-meson was first established experimentally in the reaction $\gamma p \rightarrow \pi^{o} p$. Also, nucleon resonance states such as $P_{3/2}$ $\Delta(1236)$, $D_{3/2}$ $N(1518)$, $F_{5/2}$ $N(1688)$ can be produced in photon-proton collison much in the same manner as excited states of an atom are generated by absorbing photons. When bombarding hadrons by photons to study the hadron properties, the internal structure of the hadrons is not changed measurably due to the small size of the photons. Therefore photons are also, apart from a tool to create particles, well suited as "test particles" which can "feel" the structure of hadrons and clarify the properties of strong interactions.

In recent years the Vector Dominance Model (VDM), and in particular its application to problems where the photon interacts with hadrons, "the ρ-photon analogy" (more strictly the "ρ-ω-ϕ photon analogy") has been a major stimulus to particle theory and experiment. It suggests that the photon should act generally like a hadron in high energy reactions. First

formulated by Sakurai[1] in the early 1960's, VDM treats photons as completely equivalent to a superposition of the strongly interacting vector mesons ρ^o, ω, and ϕ which have the same spin, parity and charge conjugation ($J^{PC} = 1^{--}$) as photon. The connection between the hadronic electromagnetic current J_μ^{em} and the fields of vector mesons V_μ can be expressed by the following relation:[1,2]

$$J_\mu^{em} = -\sum_V \frac{m_V^2}{2\gamma_V} V_\mu$$

where $V = \rho^o$, ω, ϕ, and m_V and γ_V are the mass and coupling parameters of the vector mesons respectively. The most important member of this group is the ρ^o meson. The assumption made here is that the vector mesons ρ^o, ω, and ϕ completely saturate the electromagnetic current.

With the advent of electron accelerators of high energies, photoproduction of mesonic resonances, in addition to nucleon resonances, became accessible. These experiments yield results of inherent interest, such as the direct photon-vector meson couplings. Photoproduction of rho mesons in the reaction $\gamma p \rightarrow \rho^o p$ has been studied by various experimenters,[3-6] showing that the ρ^o cross section is approximately constant above 2 GeV. In addition, earlier observers[5-7] of ρ^o photoproduction by unpolarized photon beams reported a lower rho mass, 20-40 MeV lower from rho production by charged pion beams. It was also pointed out that the rho shape is skewed with respect to the

p-wave Breit-Wigner resonance shape. More recent measurements on ρ^o production have been performed at DESY,[8] Cornell,[9] and SLAC[10] with polarized photons. The SLAC experiments, using bubble chamber and almost monochromatic photon beams, have resulted in a detailed study of exchange mechanisms involved in the photoproduction reactions on hydrogen. They have also observed lower ρ^o mass value and shape skewing.

So far only a few bubble chamber experiments on the coherent photoproduction of resonances in deuterium have been performed,[11,12] and thus much less data exist on the γd interactions. No group has yet tried to do a detailed photoproduction mechanism study of vector mesons produced on deuteron. In γd interactions one can study not only the coherent production of vector mesons but also γn reactions. Moreover, certain γn reaction channels whose counterparts are not accessible to bubble chamber techniques can be studied. These include, for example, $\gamma n \rightarrow p\pi^-\pi^o$ or $p\pi^+\pi^-\pi^-\pi^o$ whose counterparts $\gamma p \rightarrow n\pi^+\pi^o$ or $n\pi^+\pi^+\pi^-\pi^o$ have two neutral secondaries and thus can not be constrained. One further characteristics of photoproduction experiments in deuterium is the uniqueness of $I = 0$ exchange in the coherent γd events.

In this dissertation we present the results of a study of the reaction $\gamma d \rightarrow \rho^o d$ in the channel $\gamma d \rightarrow \pi^+\pi^- d$ at 5.5 GeV photon energy. We used the SLAC Compton back-scattered laser beam[13-15] incident on the 82" deuterium bubble chamber. This experiment has the following advantages, not all of which are

found in previous studies of multibody photoproduction on deuteron: nearly monoenergetic photon spectrum, a highly polarized beam (more than 90%), and a 4π detection efficiency provided by the bubble chamber. These unique advantages in our experiment enabled us to make a detailed analysis of the ρ^o production mechanism. We have also examined the s-channel helicity conservation and skewing of ρ^o mass shape. We have determined mass and width for ρ^o, and also obtained its production cross section in this channel.

In Chapter II we give a description of the experimental procedure and about the photon beam. Chapter III is devoted to the parameterization and fitting to the ρ^o resonance shape, whereas the study of production and decay of the ρ^o meson is presented in Chapter IV. The determination of ρ^o production cross section is given in Chapter V, and our results are compared with those obtained in previous works.[12] We also investigate in this Chapter a few other channels for the production of ω, ϕ, ρ', and A_1 mesons. Finally our results and conclusions are summarized in Chapter VI.

II. EXPERIMENTAL DETAILS

The data for this study comes from a high statistics experiment performed at the Stanford Linear Accelerator Center (SLAC). The deuterium filled 82" bubble chamber was exposed to a nearly monoenergetic linearly polarized photon beam of 5.5 GeV. A total of 501,888 pictures were taken over three separate periods of time from May 1971 to February 1972.

A. Photon Beam

The experiment utilized a polarized monochromatic photon beam produced by back-scattering a polarized ruby laser beam from the 17.5 GeV SLAC electron beam. This scheme was first suggested, in 1962, by Milburn[16] of U.S.A. and concurrently by Arutyunian *et al.*[17] of Russia. They pointed out that backward Compton scattering of polarized laser light by high energy electrons would produce high energy polarized monochromatic photon beams.

Since Compton scattering is a two-body process, the final energy of the photon depends uniquely on its laboratory scattering angle θ (Fig. 1a). If the energies of the incoming photon and electron are K (=1.786 eV) and E respectively, then the scattered photon energy is given by[13]

$$K' \approx \frac{K'_m}{1 + (E\theta/E_c)^2}$$

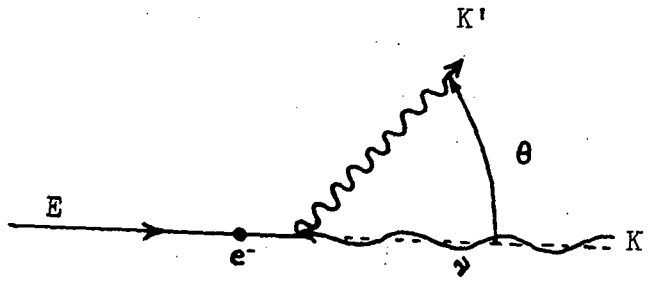
K'
θ
E
e⁻
γ
K

(a)

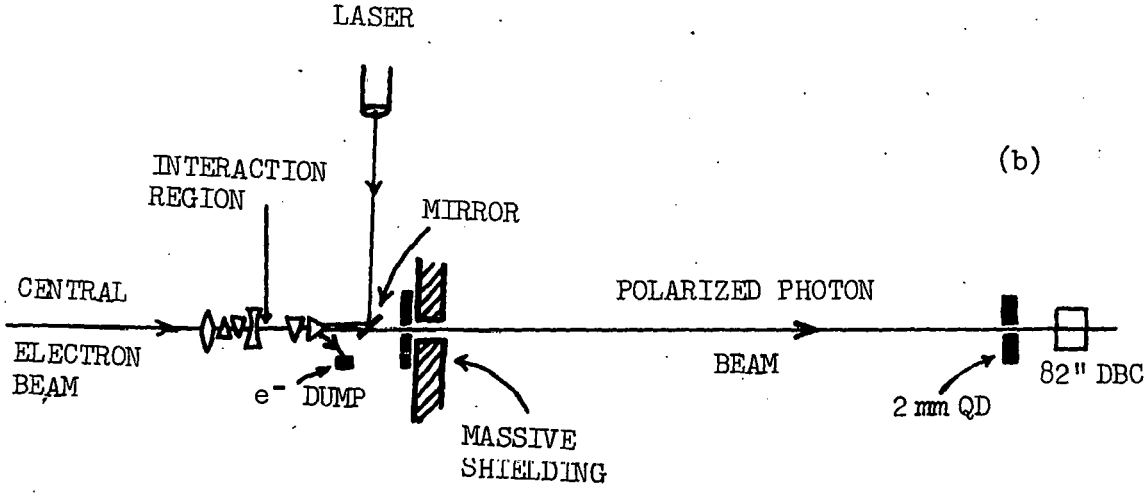
LASER
INTERACTION
REGION
MIRROR
CENTRAL
ELECTRON
BEAM
e⁻ DUMP
POLARIZED PHOTON
BEAM
MASSIVE
SHIELDING
2 mm QD
82" DBC

(b)

Fig. 1

where E_c is the total center of mass energy and $K_m' = 4E^2K/E_c^2$.

If the incident laser light is linearly polarized, the scattered photons retain most of the linear polarization for 180^o scattering. Also the energy and polarization of the back-scattered beam are determined by its collimation angle.

Figure 1b shows a simplified beam schematic layout. The incident laser light was made linearly polarized by using a Brewster stack. The plane of polarization could be rotated 90^o by inserting a half-wave plate into the beam line. This linearly polarized laser light then collides with the electron beam at a relative angle of 3 milli-radians. The electron beam was deflected and dumped after collision.

The back-scattered energetic photon beam, before entering the bubble chamber, passes through a collimator QD. This collimator[15] consists of four scintillation counters surrounding a 2 mm diameter hole through 6" of Hevimet. The signals from these counters were used to control the electron beam steering to about 10^{-6} radians, and to monitor the photon beam intensity. Control of the intensity was accomplished by adjusting the laser output or the electron beam intensity. More details about the beam are given in Ref. 18.

B. Scanning and Measuring Procedures

The purpose of the scan was to find the hadronic interactions (hereafter referred as events) and to determine the photon flux entering the bubble chamber. An event was defined

as a number of out going particles, such as deuteron, proton, pion, kaon, etc., produced due to strong-interaction from a gamma-deuteron collision. Neutral strange-particle events are recognized by their decay signature (V). Main background to events consists of electron-positron pairs, produced by electromagnetic interactions, which reduced visibility near the beam line. These pairs had minimum bubble density, zero opening angle and even charge balance, and pointed in the beam direction. In contrast, most hadronic events had some tracks with heavier ionization than e^+e^- tracks, with dip and azimuth angles different from the beam direction, and were easily identified from the pair background.

All the film was scanned for events with two and more out going charged tracks (prongs). The events with neutral strange-particle decays with one or two V topology (for studying K^o decays to check energy determination) were also recorded. Each production vertex and V vertex, if present, were rough-digitized as input for later measurements on LBL Cobweb Data Reduction System.[19] The electron-positron pairs were also counted on two frames in sequence beginning on frame 50 and separated by 50 frames, i.e. 50, 51, 100, 101 etc., on each roll of film of about 875 frames. The events scans and the pair counts were performed in the same fiducial area, which is well-defined on the film as the diameter of the photon beam is less than 3 mm in space. We scanned only 157 cm fiducial length in order to allow at least 35 cm of

measurable length for forward tracks and about 15 cm for backward tracks (all dimensions in chamber space).

Two third of the film was double-scanned at U. C. Riverside, and the remaining one third was scanned at LBL. The combined scan efficiency was found to be greater than 99% for topologies with three or more prongs. The scanning efficiency for two-prong events was found to be (90 ± 3)%. This lower value is due to the fact that two-prong events with small opening angles are often misidentified as e^+e^- pairs by the scanners. This, however, has a negligible effect on the total number of pairs used in determining the incoming photon flux.

A total of 34,891 events, for two to seven out going charged tracks, were found (Table 1). These events exclude 1,740 events with neutral strange-particle decays. The average number of e^+e^- pair counts was 6.326 pairs per frame. The scanning information was recorded on magnetic tapes for input to the Cobweb system.

The Cobweb system is a on-line computer-controlled (IBM 7044) automatic measuring machine. It is designed to improve and increase the measuring rate of conventional track-following Franckensteins. The computer not only collects and records the measurement output from the two Franckensteins, but also monitors and checks their operations. This system uses the scanning information recorded on the input tape to position the events for measurement. The operator measures

TABLE 1

Topological events' statistics

Topology	Total Scanned Events	Unmeasurable Events	Poorly Measured Events	No Fits
2 - prong	6917	548	106	331
3 - prong	16753	1195	1042	1001
4 - prong	3661	278	205	340
5 - prong	6278	525	548	643
6 - prong	579	35	66	88
7 - prong	703	56	95	87

each track in a single view, the computer driving the stage back to the vertex after each track is complete. A curve is fitted separately to each track in each view to check the accuracy of measurement. The vertex point is taken only once in each view, but that point is used in the fit for all tracks from that vertex. If the track does not pass the curve-fitting-check the operator must remeasure the vertex.

The measurement informations for successfully measured events were recorded on magnetic tapes. The number of events that could not be measured due to secondary scatters or track obscuration are given, according to topologies, in Table 1 under the heading 'Unmeasurable Events'. These are 8% of the total scanned events.

C. Kinematical Reconstruction

All the measured events, including neutral strange-particle decays and e^+e^- pairs, were processed through the kinematics reconstruction and hypothesis fitting program SIOUX (TVGP and SQUAW). For data processing we used COPE terminal at UCR connected to LBL CDC-7600 computer system. For two to five out going charge particle topologies, the fit hypotheses made in SQUAW are given in Table 2. Events with an even number of prongs (with an unseen positive track) were fitted assuming the missing track to be either an impulse proton or a recoiled deuteron. In both cases the momentum of the track was taken to be zero, and the errors assigned

TABLE 2

Number of events fitted to different hypotheses (not uniquely) for the fitted photon energy within the range 4.7 - 6.2 GeV

Hypothesis	Number of Constraints	Number of events fitted when visible tracks are			
		2	4	3	5
$\gamma d \rightarrow \pi^- pp$	3	26		18	
$\rightarrow \pi^- pp\pi^o$	0	1305		2777	
$\rightarrow \pi^- \pi^+ pn$	0	1563		3620	
$\rightarrow \pi^- \pi^+ d$	3	702		474	
$\rightarrow \pi^- \pi^+ d\pi^o$	0	-		2767	
$\rightarrow k^- k^+ d$	3	465		88	
$\rightarrow k^- k^+ pn$	0	1724		4046	
$\gamma d \rightarrow \pi^- \pi^- \pi^+ pp$	3		374		149
$\rightarrow \pi^- \pi^- \pi^+ pp\pi^o$	0		1028		1681
$\rightarrow \pi^- \pi^- \pi^+ \pi^+ pn$	0		987		1882
$\rightarrow \pi^- \pi^- \pi^+ \pi^+ d$	3		10		75
$\rightarrow \pi^- \pi^- \pi^+ \pi^+ d\pi^o$	0		-		1384

to the momentum were $\Delta P_x = \Delta P_y = 0.75 \Delta P_z = \pm$ 30 MeV/c for an unvisible proton and $\Delta P_x = \Delta P_y = 0.8 \Delta P_z = \pm$ 40 MeV/c for a missing recoil deuteron. The larger error in P_z compensates for the increased uncertainty due to the difficulty in seeing steep tracks in Z-direction which is the optical axis. The difference in the errors reflects the fact that proton of momentum less than 80 MeV/c leaves no visible track in the bubble chamber, while a deuteron must have a minimum momentum of about 110 MeV/c to be visible.

The fits assumed that the beam momentum was unknown, that is, no constraint was placed on the incident photon momentum. Whereas, the photon beam was assigned dip (-0.3°) and azimuth (93.1°) angles as determined from the measurements of e^+e^- pairs. Consequently, hypotheses with no missing neutral had three kinematic constraints (3C) and those with one neutral had no constraint (OC). All three-constraint fits were required to have kinematic chi-square less than 26.

Thirteen percent of the total scanned events could not pass the SIOUX processing. The number of these failing-events are given in last two columns of Table 1 (number of events under the heading 'Poorly Measured Events' could not pass TVGP, whereas events in the last column could not pass SQUAW) according to topologies. The number of events which passed SIOUX and fitted to various hypotheses are given in Table 2. Both unique and ambiguous fits to different hypotheses are included.

The reconstruction procedure and the accuracy of bubble chamber magnetic field value (used in fitting programs) were checked and corrected by fitting all $K^{o} \rightarrow \pi^{+}\pi^{-}$ decays with unconstrained mass. As shown in Fig. 2, the $\pi^{+}\pi^{-}$ mass-resolution at the K^{o} mass value of 497.8 MeV was ± 6 MeV, and the mass of K^{o} is correct to 0.8%.

D. Energy Spectrum and Polarization of the Photon Beam

Since the data were collected in three separate periods of time, the energy spectra of photon beam were examined separately in three batches. Figure 3 shows the photon energy spectra obtained from the measurement and fitting of $e^{+}e^{-}$ pairs. The top energy spectrum is the combination of the three spectra. The energy spectra peak at ≈ 5.5 GeV and have average value of full width at half maximum of 0.6 GeV. For subsequent analysis of events we do not include the low-energy tail of the photon spectrum, $E_{\gamma} < 4.7$ GeV, which contains about 18% of the photons.

The linear polarization of the photon beam can be calculated using the formalism of Murray and Klein.[13] Using the spectra of Fig. 3 we calculated the average value of linear polarization of the photon beam as (91 ± 2)% of the original 100% laser light polarization. Uncertainties are introduced in the polarization direction of the back-scattered photon beam at the bubble chamber due to the alignment and transportation of the laser light. Although the polarization

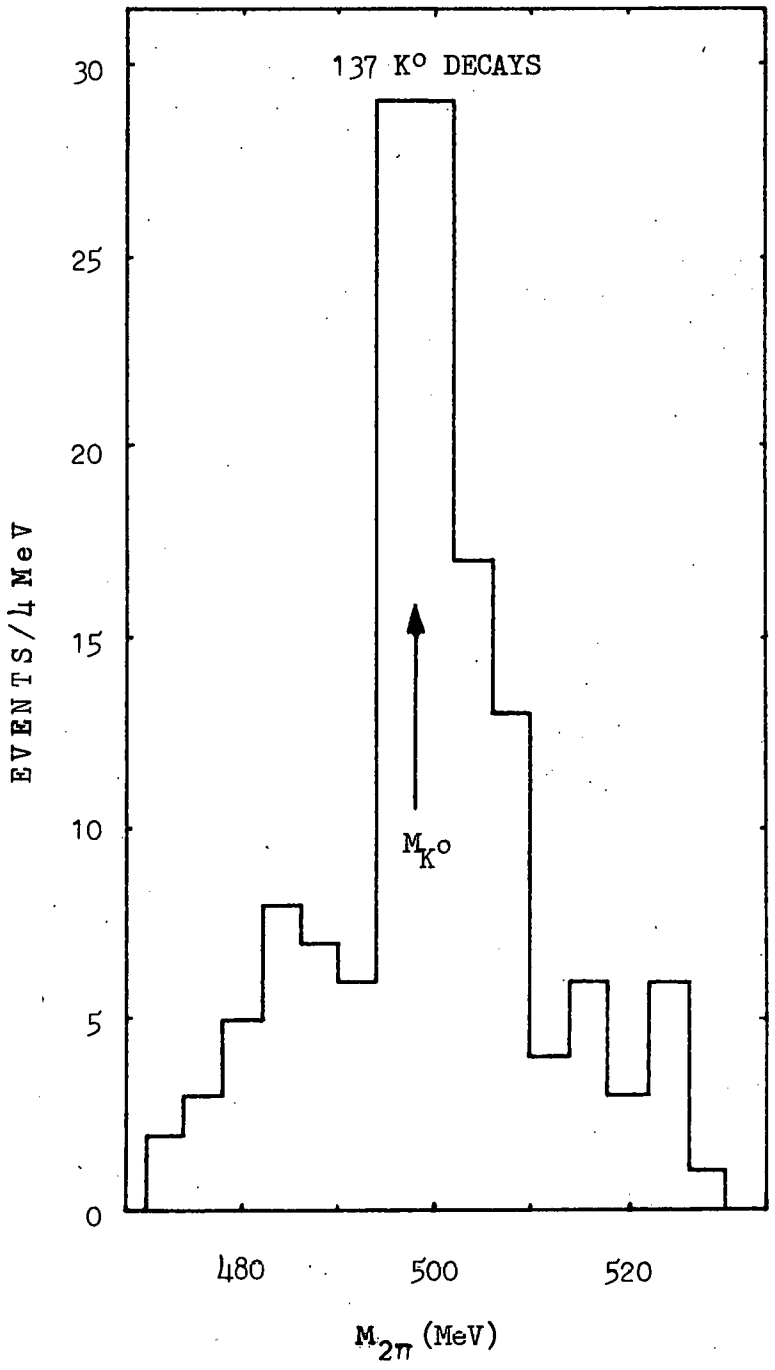
137 K° DECAYS
30
25
20
15
10
5
0
EVENTS/4 MeV
M_{K^0}
480
500
520
$M_{2\pi}$ (MeV)

Fig. 2

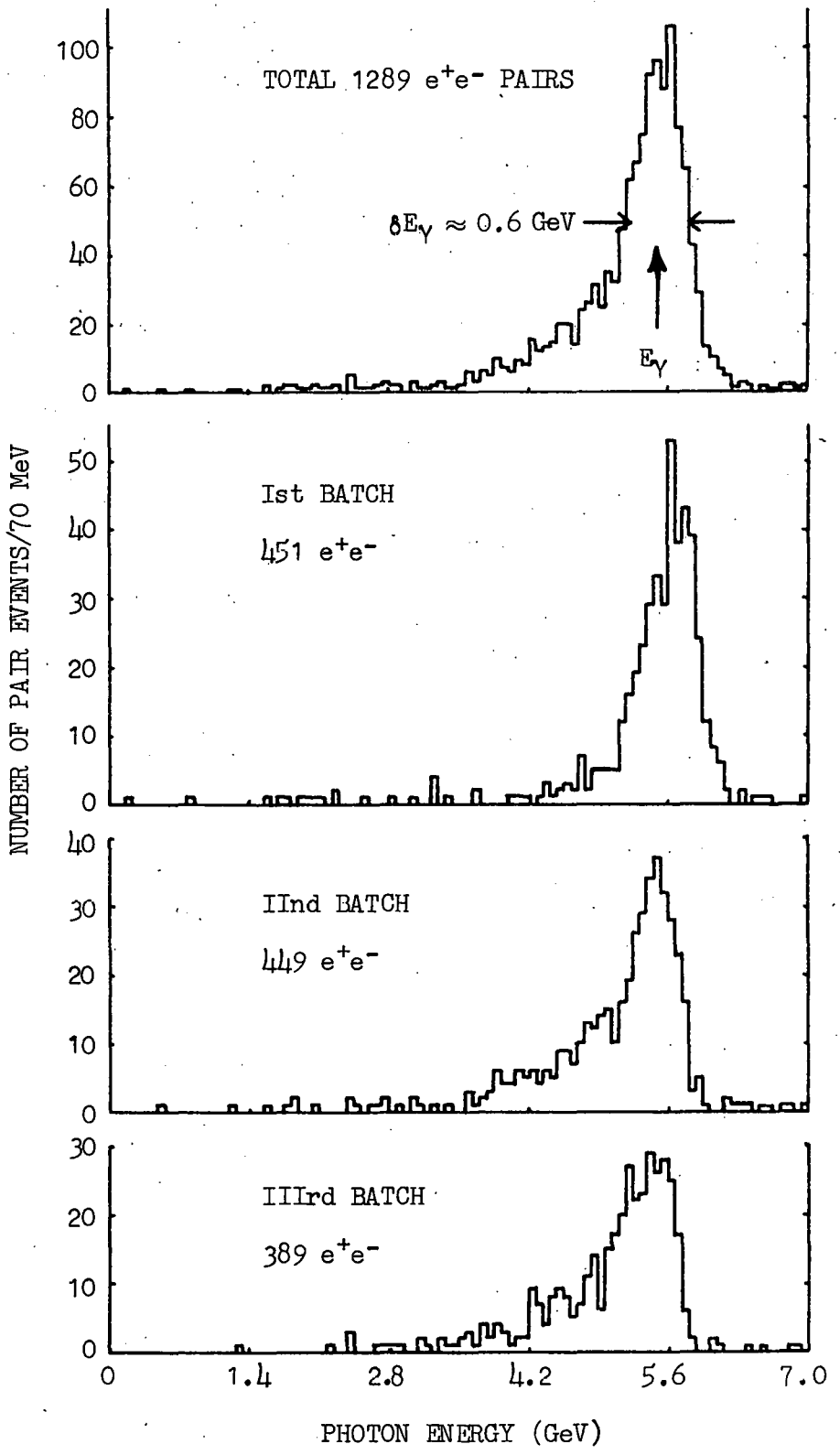
TOTAL 1289 e+e- PAIRS
δEγ ≈ 0.6 GeV
Eγ
Ist BATCH
451 e+e-
IInd BATCH
449 e+e-
IIIrd BATCH
389 e+e-
NUMBER OF PAIR EVENTS/70 MeV
PHOTON ENERGY (GeV)
0
1.4
2.8
4.2
5.6
7.0

Fig. 3

direction was measured to an accuracy of 1^{o} at the laser, the overall uncertainty in the polarization direction is $\pm 3^{o}$ at the bubble chamber.

III. FITTING PROCEDURE FOR THE REACTION $\gamma d \rightarrow \pi^+\pi^- d$

In the kinematic analysis of two and three prong events, no constraint was placed on the incident photon momentum and the following final state hypotheses were considered:

(a) Three-constraint reactions

(1) $\gamma\ d \rightarrow \pi^+\ \pi^-\ d$

(2) $\gamma\ d \rightarrow \pi^-\ p\ p$

(3) $\gamma\ d \rightarrow K^+\ K^-\ d$

(b) Zero-constraint reactions

(1) $\gamma\ d \rightarrow \pi^+\ \pi^-\ p\ n$

(2) $\gamma\ d \rightarrow \pi^-\ \pi^o\ p\ p$

(3) $\gamma\ d \rightarrow \pi^+\ \pi^-\ \pi^o\ d$

(4) $\gamma\ d \rightarrow K^+\ K^-\ p\ n$

From the 16,753 (6,917) scanned events we found 365 (603) three (two) prong events which gave 3C fits to the reaction

$$\gamma\ d \rightarrow \pi^+\ \pi^-\ d \qquad \ldots\ldots\ (1)$$

with fitted photon energy, E_γ, in the interval $4.7 \leq E_\gamma \leq 6.2$ GeV and $\chi^2 \leq 15$. Due to the low binding energy of the deuteron, coherent deuteron reactions are characterized by a steeply decreasing momentum transfer distribution. Since deuterons with $P < 110$ MeV/c are undetected on the film, a large fraction of the coherent events will thus have an invisible deuteron

(two-prong topology). These events will generally also pass the corresponding 0C fit with an out going proton and neutron ($\gamma d \rightarrow \pi^+ \pi^- p_s n$). However, if the event is really a coherent one, the fitted proton and neutron both will be moving nearly in the same direction and their invariant mass will be enhanced in the region of the deuteron mass. By inspecting, therefore, the final state $\gamma d \rightarrow \pi^+\pi^- p_s n$ fits and requiring $M(p_s n) \leq 1.885$ GeV we expect the two-prong sample to be free of background.

For our ρ^o study we accepted only those two-prong events which had $|t_{min}| = 0.003 \leq |t| \leq 0.025$ GeV^2 and which also fitted to the hypothesis $\gamma d \rightarrow \pi^+\pi^- p_s n$ with $M(p_s n) \leq 1.885$ GeV, and those three-prong events which had $|t| > 0.025$ GeV^2. Here t is the square of the four-momentum transfer from incoming photon to the dipion mass. In this reaction the minimum momentum transfer is 0.003 GeV^2, and $|t| > 0.025$ GeV^2 corresponds to deuteron track lengths of greater than 2 mm in the bubble chamber and nearly all are three-prong events with a measured d track. The t-distribution for the sample of 775 events thus obtained is shown in Fig. 4. The coherent ρ^o production forward peak is clearly seen.

A. Mass Distributions

Figure 5 shows the $\pi^+\pi^-$ effective mass distributions for the reaction (1). The top spectrum is for all the events; below, these distributions are repeated for events grouped

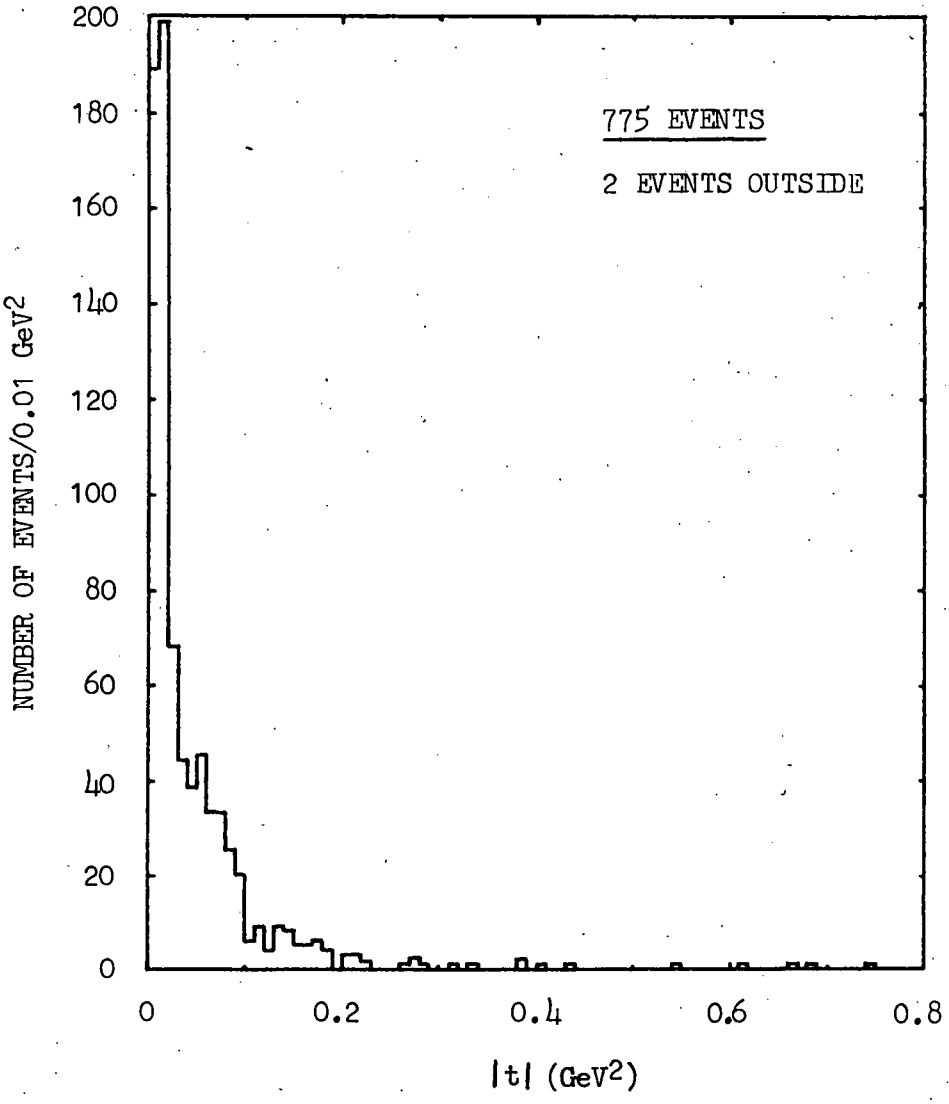
775 EVENTS
2 EVENTS OUTSIDE
NUMBER OF EVENTS/0.01 GeV²
200
180
160
140
120
100
80
60
40
20
0
0
0.2
0.4
0.6
0.8
|t| (GeV²)

Fig. 4

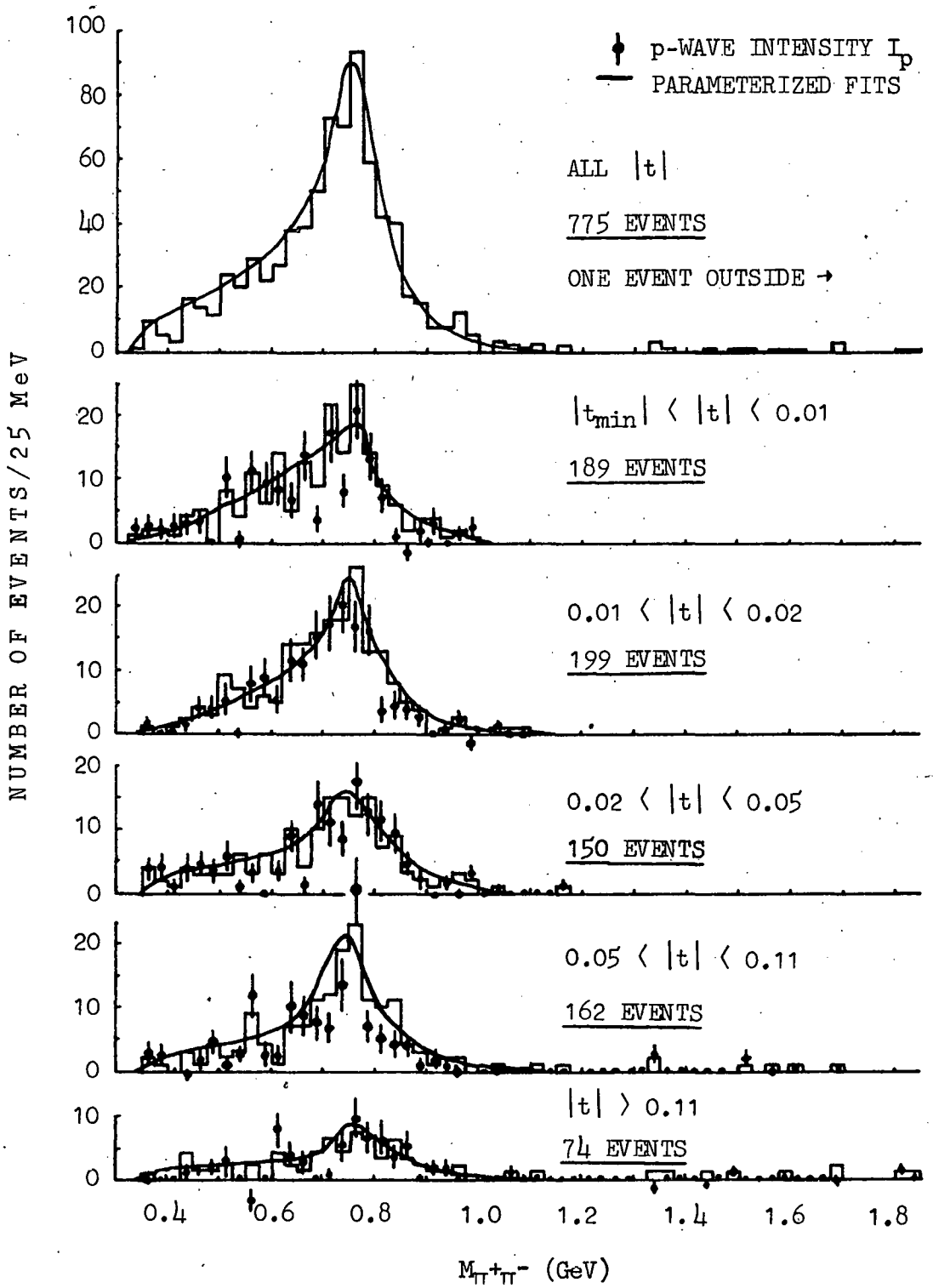
p-WAVE INTENSITY I_p
PARAMETERIZED FITS
ALL |t|
775 EVENTS
ONE EVENT OUTSIDE →
$|t_{min}| < |t| < 0.01$
189 EVENTS
$0.01 < |t| < 0.02$
199 EVENTS
$0.02 < |t| < 0.05$
150 EVENTS
$0.05 < |t| < 0.11$
162 EVENTS
$|t| > 0.11$
74 EVENTS
NUMBER OF EVENTS/25 MeV
$M_{\pi^+\pi^-}$ (GeV)

Fig. 5

into various t-intervals. The ρ^o production is observed in these $\pi^+\pi^-$ mass distributions. It is clear from the Fig. 5 that ρ^o does not peak at commonly accepted ρ^o mass,[3,4,20,21] but at lower value near 750 MeV, does not have the shape of a p-wave Breit-Wigner,[3] and changes shape as a function of t.[10]

In Fig. 6 we have shown the $\pi^{\pm}d$ effective mass distributions to study the production of d*. The πd mass distributions, however, show no d* enhancement near M(πd) = 2.2 GeV as reported in some πd and Kd experiments.[22,23]

B. Parameterization

Hilpert et al.,[12] in the reaction $\gamma d \rightarrow \pi^+\pi^- d$, obtained reasonable fits to the $\pi^+\pi^-$ mass distributions. They multiplied the Breit-Wigner distribution with an energy dependent width (according to Jackson[24]) for the ρ^o by a mass-skewing factor $(M/M_{\pi\pi})^4$ from the diffraction dissociation model of Ross and Stodolsky.[25] However, in a study[10] of reaction $\gamma p \rightarrow \pi^+\pi^- p$ it has been concluded that the ρ^o Breit-Wigner should be multiplied by $(M/M_{\pi\pi})^{n(t)}$; the parameter n(t) is greater than 5 near t = 0 but drops to zero around -t = 0.5 GeV^2. In the absence of any precise theory of the line shape of broad resonance like the ρ^o, we made maximum-likelihood fits to the events of the reaction (1) assuming the density distribution of events as

$$dP = \left[a_\rho . BW_\rho(M_{\pi\pi}) . W(\cos\theta_H) . (M_o/M_{\pi\pi})^{n(t)} . e^{A_\rho t} + a_{PS} \right] d(PS) \quad \ldots(2)$$

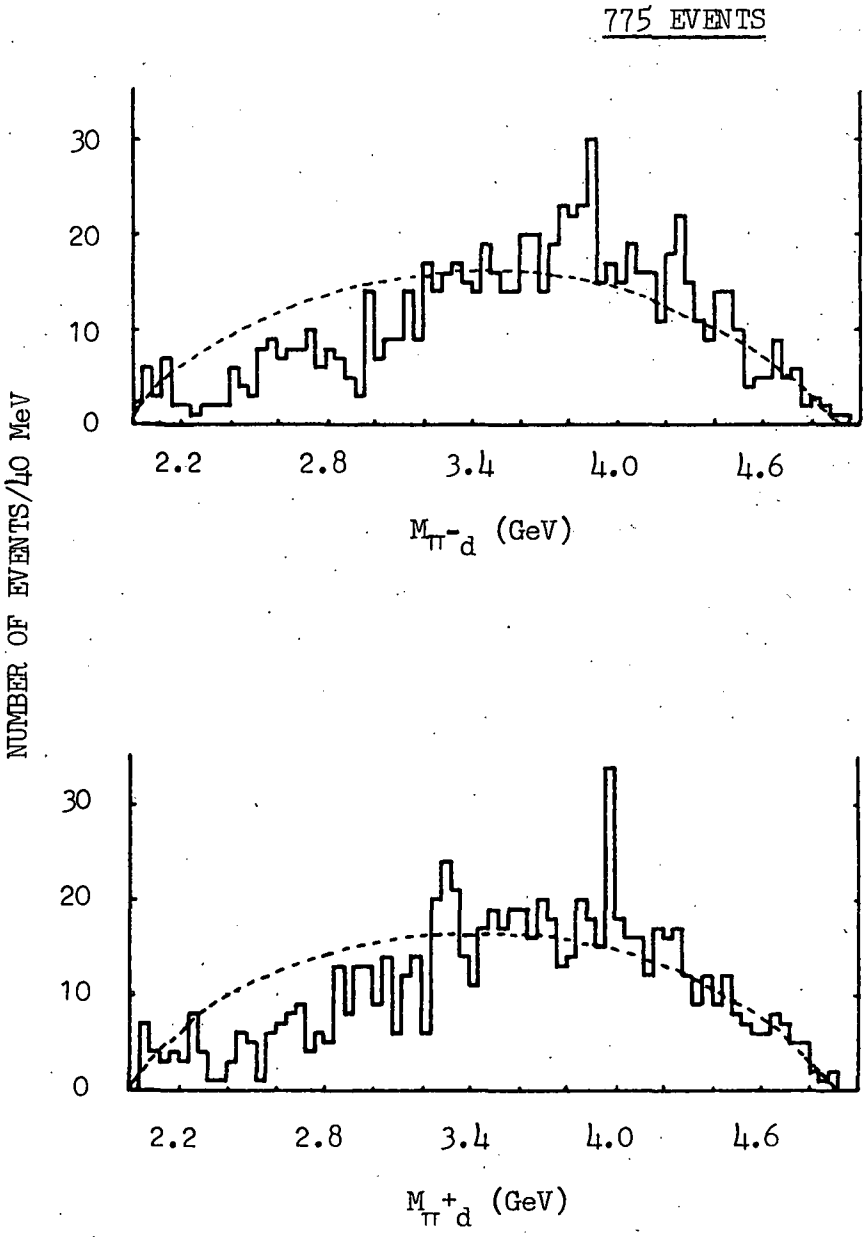
775 EVENTS
NUMBER OF EVENTS/40 MeV
30
20
10
0
2.2
2.8
3.4
4.0
4.6
$M_{\pi^- d}$ (GeV)
30
20
10
0
2.2
2.8
3.4
4.0
4.6
$M_{\pi^+ d}$ (GeV)

Fig. 6

where $$BW_\rho(M) = \frac{M}{q(M)} \cdot \frac{M_o\Gamma}{(M^2 - M_o^2)^2 + M_o^2\Gamma^2}$$

$$\Gamma = \Gamma_o\left[\frac{q(M_{\pi\pi})}{q(M_o)}\right]^3 \cdot \frac{f(M_{\pi\pi})}{f(M_o)}$$

$$f(M) = \left[q^2(M) + q^2(M_o)\right]^{-1}$$

a_ρ, a_{PS} = fraction of ρ^o production and phase space background (apart from suitable normalization factors)

$q(M)$ = three-momentum of the pion in the $\pi^+\pi^-$ rest system

$W(\cos\theta_H) = 3/4 \cdot \sin^2\theta_H$ describes the experimentally observed ρ^o decay angular distribution in the helicity frame

M_o, Γ_o, $n(t)$, A_ρ = paramerters of the fit.

C. OPTIME Program

Computer program OPTIME, developed at Lawrence Berkeley Laboratory[26] allows the user to fit a mathematical expression to a set of experimental data by maximum-likelihood method. Let there be N experimental events and each event be specified completely by n quantities which are considered to be the components of a vector $\hat{\xi}$. For kth event, if $\hat{x}$ is a particular value which $\hat{\xi}_k$ can take, then the contents of a hypervolume $d\hat{x}$ centered around $\hat{x}$ is a random variable $\gamma(\hat{x}, d\hat{x})$. The expectation value of this random variable, $y(\hat{x})$ is then the true distribution of events. However, this function $y(\hat{x})$ is not known; we therefore assume a known function $Y(\hat{x}, \hat{a})$,

where $\hat{a}$ is a vector of N_a components, and that there exists a set of parameters $\hat{A}$ such that:

$$Y(\hat{x}, \hat{A}) = y(\hat{x})$$

where the vector $\hat{A}$ with components A_j is called the true value of the parameter $\hat{a}$. The purpose of the OPTIME fit is to find an estimate $\hat{\alpha}$ for $\hat{A}$ such that

$$Y(\hat{x}, \hat{\alpha}) \approx y(\hat{x})$$

The user supplies a function with m variable parameters. OPTIME is a stepping process, adjusts the parameter such that the sum of the logarithums of the function over all data points reaches a maximum. If the function is unnormalized, as in our case, integration data points are generated by the Monte Carlo program SAGE[27] (a set of subroutine in OPTIME). SAGE generated events can be made to resemble as closely as possible the function to be integrated by coding various subroutines.

The output of OPTIME constitutes the parameters $\hat{\alpha}$. To check the fit, histograms are prepared using the function $Y(\hat{x}, \hat{\alpha})$ and are compared with the experimental distribution of the events.

D. Fitting Procedure

We first determined M_o, Γ_o, n(t), and A_ρ from an overall fit in the region $-t < 0.11$ GeV^2. With M_o, Γ_o, and A_ρ fixed at these values, the quantities a_ρ, a_{PS} and the final value

of n(t) were fitted for different t-intervals (see Table 3). The fits described the $\pi^+\pi^-$ mass spectra well, as shown by the curves in Fig. 5. The fitted values of n(t) are shown in Fig. 7. Over the accessible t-range in this experiment the value of n(t) is in agreement with the findings of the previous study.[10]

In Fig. 8 we display the curves corresponding to n(t) = 4 and the best fitted value of n(t) = 4.93 for the region $-t < 0.11$ GeV^2. The solid line gives the fit result of n(t) = 4.93 with confidence level $\approx$25% and is far better than that obtained with the factor n(t) = 4 shown as a dashed line (confidence level less than 0.1%).

In the lowest four t-bins (t_{min} - 0.11 GeV^2), which contains about 90% of the accepted events of reaction (1), we obtained from the fit for the rho mass and width the values (766 ± 5) and (139 ± 11) MeV, respectively. The value obtained for the exponential slope, A_ρ, was (35.1 ± 1.6) GeV^{-2}.

TABLE 3

Values of n(t) and event distribution at different t-intervals

$\|t\|$ GeV^2	n(t)	Number of events under	
		rho peak	phase space
t_{min}-0.01	3.6±1.1	95.6±15.6	93.4±16.0
0.01-0.02	4.7±0.5	183.6±16.9	15.8± 7.0
0.02-0.05	5.5±0.4	145.6±15.0	4.4± 4.6
0.05-0.11	4.5±0.6	150.2±14.0	11.8± 4.7

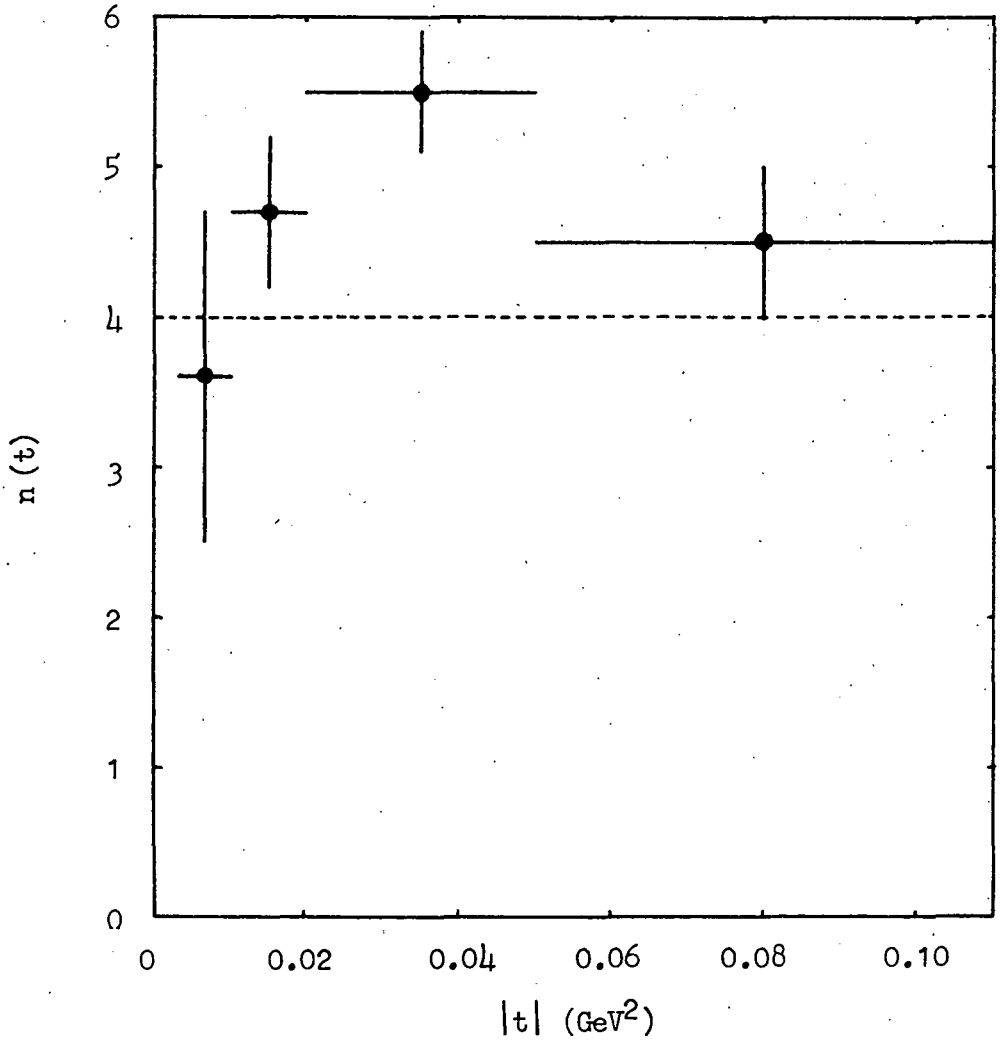

Fig. 7

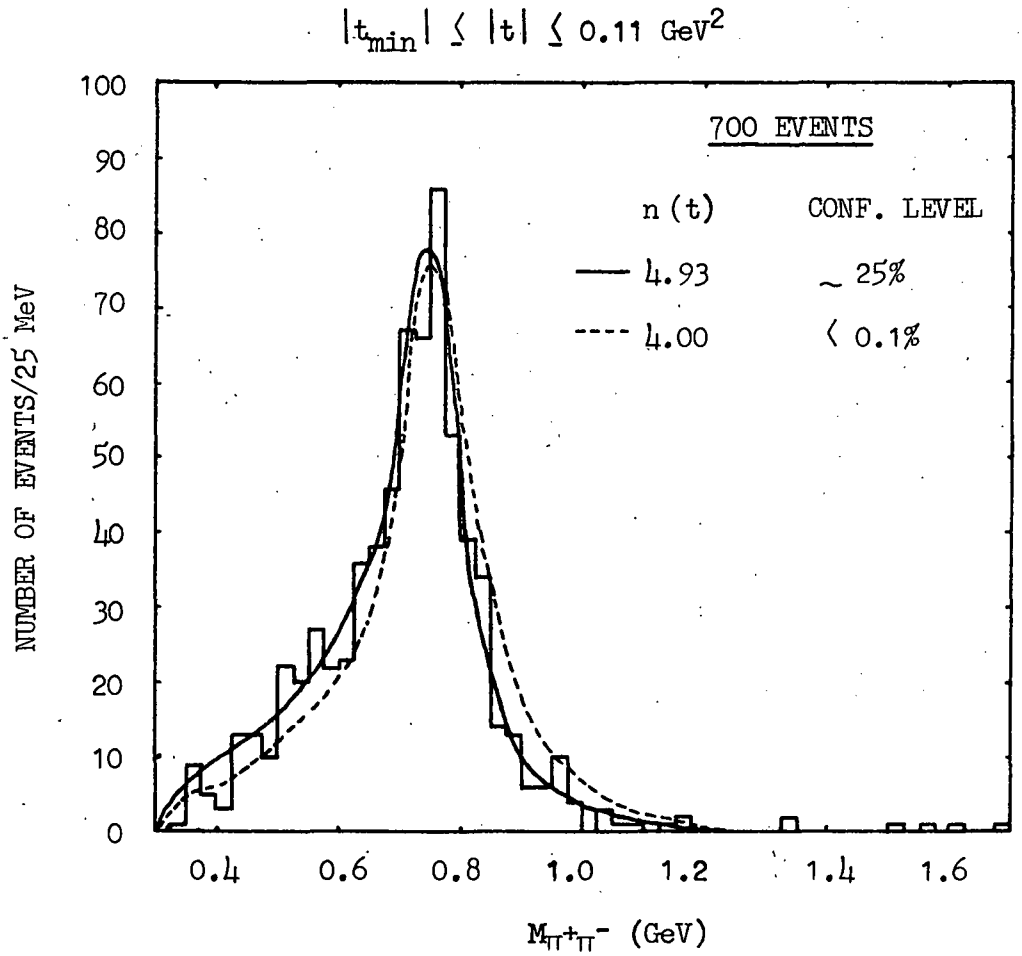
$|t_{min}| \leq |t| \leq 0.11$ GeV^2
700 EVENTS
n (t)
CONF. LEVEL
4.93
~ 25%
4.00
< 0.1%
NUMBER OF EVENTS/25 MeV
100
90
80
70
60
50
40
30
20
10
0
0.4
0.6
0.8
1.0
1.2
1.4
1.6
$M_{\pi^+\pi^-}$ (GeV)

Fig. 8

IV. COHERENT ρ^o PHOTOPRODUCTION ON DEUTERON

In this chapter we discuss the angular distribution of $\pi^+\pi^-$ in their rest system. It will be shown below that the $\pi^+\pi^-$ pairs are in a predominantly p-wave state, so for brevity we refer to them as ρ^o.

A. Analysis of Dipion Angular Momentum States

The full description of vector meson photoproduction requires 12 complex amplitudes, or 23 real numbers at a given energy and momentum transfer. With the polarized beam and using the full decay angular distribution of vector meson it is possible to measure 10 (nine parameters of decay spin-density matrix and the diffraction cross section) of the 23 parameters. Whereas only 4 of these parameters can be determined with unpolarized beams.

We use the formalism of Schilling et al.[28,29] for the analysis of ρ^o decay angular distribution produced by linearly polarized photons. The results are presented in three frames, namely, helicity (H), Gottfried-Jackson (G-J), and Adair (A) frames. The three frames differ in the choice of the Z-axis, the spin quantization axis. The helicity frame has its Z-axis in the direction of the ρ^o in the overall (Yd) c.m. system, the Adair frame in the direction of the incident photon in the overall c.m. system, and the G-J frame in the direction of the incident photon in the ρ^o rest system. In

all these systems the Y-axis is taken as the normal to the production plane. For forward produced ρ^o mesons, all the three systems coincide.

In all three systems the decay angular distribution for ρ^o can be expressed in terms of nine independent and measureable density matrix parameters $\rho^{\alpha}_{\lambda\lambda'}$ (see Appendix A). Let Φ be the angle between the photon polarization vector, $\vec{\epsilon}_\gamma$, and the production plane, and θ and ϕ be the polar and azimuthal angles of the vector $\vec{\epsilon}_{\pi^+}$ in the ρ^o rest system (Fig. 9). Then for the degree of linear polarization of the photon to be P_γ, rho meson decay angular distribution is given as[29]

$$W(\cos\theta,\phi,\Phi) = \frac{3}{4\pi}\left\{\frac{1}{2}(1-\rho^o_{00}) + \frac{1}{2}(3\rho^o_{00}-1)\cos^2\theta - \sqrt{2}\mathrm{Re}\rho^o_{10}\cdot \sin2\theta\cos\phi - \rho^o_{1-1}\sin^2\theta\cos2\phi - P_\gamma\cos2\Phi\left[\rho^1_{00}\cos^2\theta + \rho^1_{11}\sin^2\theta - \sqrt{2}\mathrm{Re}\rho^1_{10}\sin2\theta\cos\phi - \rho^1_{1-1}\sin^2\theta\cos2\phi\right] - P_\gamma\sin2\Phi\left[\sqrt{2}\mathrm{Im}\rho^2_{10}\sin2\theta\sin\phi + \mathrm{Im}\rho^2_{1-1}\sin^2\theta\sin2\phi\right]\right\} \quad \ldots\ldots\ (3)$$

Here $\rho^o_{\lambda\lambda'}$ are the density matrix elements for the unpolarized photons, whereas, $\rho^1_{\lambda\lambda'}$ and $\rho^2_{\lambda\lambda'}$ are due to the photon's linear polarization.

Let Ψ $(= \phi - \Phi)$ be the angle between the $\vec{\epsilon}_\gamma$ and the projection of $\vec{\epsilon}_{\pi^+}$ on to a plane perpendicular to the direction of the incident photon. Then for ρ^o photoproduction in the near forward direction, the ρ^o decay distribution in the

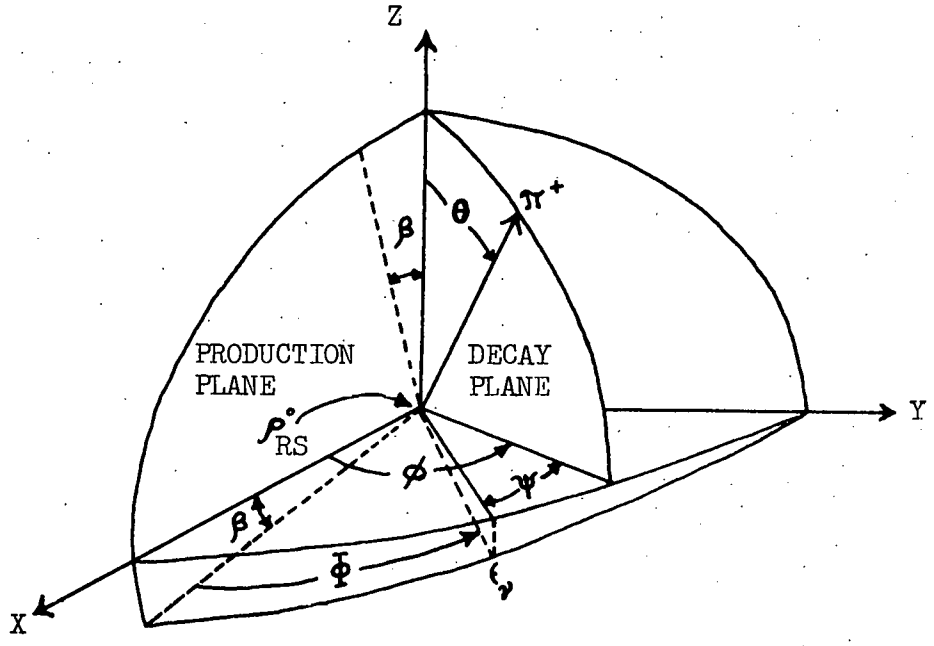
Z
Y
X
PRODUCTION
PLANE
DECAY
PLANE
β
θ
π+
ρ°RS
φ
ψ
Φ
ε

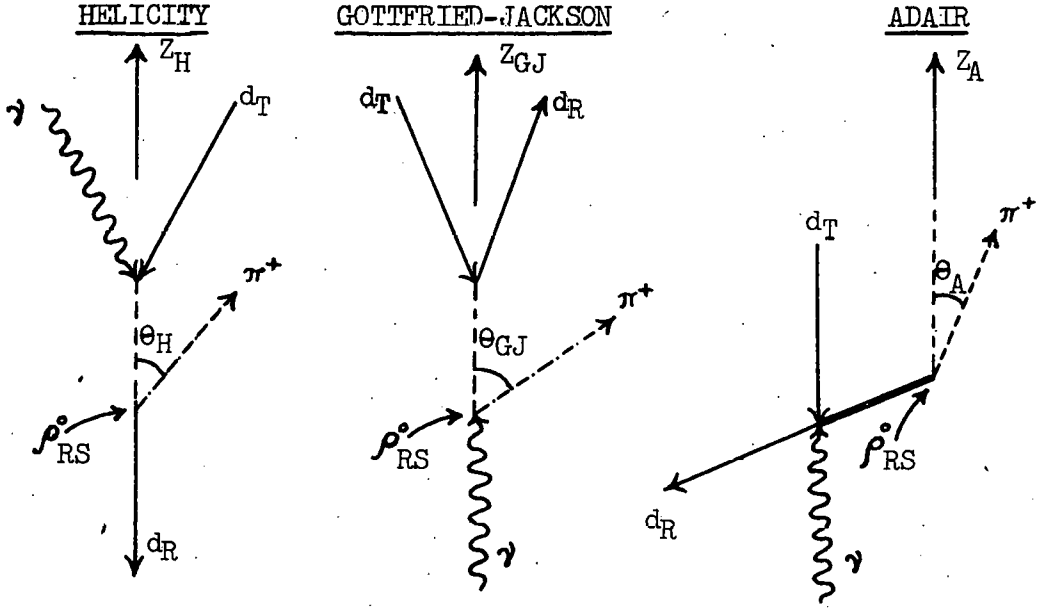
HELICITY
ZH
dT
γ
π+
θH
ρ°RS
dR
GOTTFRIED-JACKSON
ZGJ
dT
dR
π+
θGJ
ρ°RS
γ
ADAIR
ZA
dT
π+
θA
ρ°RS
dR
γ

Fig. 9

helicity frame is[10]

$$W(\theta,\Psi) = \frac{3}{8\pi} \sin^2\theta_H \, (1 + P_\gamma \cos 2\Psi_H) \quad \ldots\ldots\ldots (4)$$

The decay angular distribution of $\pi^+\pi^-$ system for events in the rho mass region, $0.6 \leq M_{2\pi} \leq 0.85$ GeV, and for small momentum transfer, $|t| \leq 0.15$ GeV^2, from this experiment are shown in Fig. 10. The $\cos\theta_H$ distribution is compatible with $\sin^2\theta_H$, consistent with complete helicity conservation at $\gamma\rho$ vertex. The Ψ_H distribution data also shows an excellent agreement with $(1 + P_\gamma \cos 2\Psi_H)$ curve ensuring that the ρ^o is almost completely linearly polarized. It is an overwhelming evidence for natural J^P exchange in ρ^o production in our experiment. The scatter plot of Ψ_H vs. $\cos\theta_H$ is proportional to $\sin^2\theta_H \times (1 + P_\gamma \cos 2\Psi_H)$ and there is no evidence of any correlation between Ψ_H and $\cos\theta_H$.

In Fig. 11 we present the moment sums, $\Sigma \mathrm{Re} Y_1^m(\theta,\Psi)$, of the $\pi^+\pi^-$ system in the helicity frame as a function of $\pi^+\pi^-$ mass for $-t \leq 0.15$ GeV^2. There are strong Y_2^o and Y_2^2 moments present in the ρ^o region which follow the asymmetric shape. The Y_2^o moment shows the behavior expected for the $\sin^2\theta$ decay of ρ^o. No significant moments, other than those associated with a p-wave system, exit in the ρ^o region indicating a negligible incoherent background in the ρ^o region.

B. Density Matrix Elements of the ρ^o States

If s-channel helicity were conserved in ρ^o photoproduction

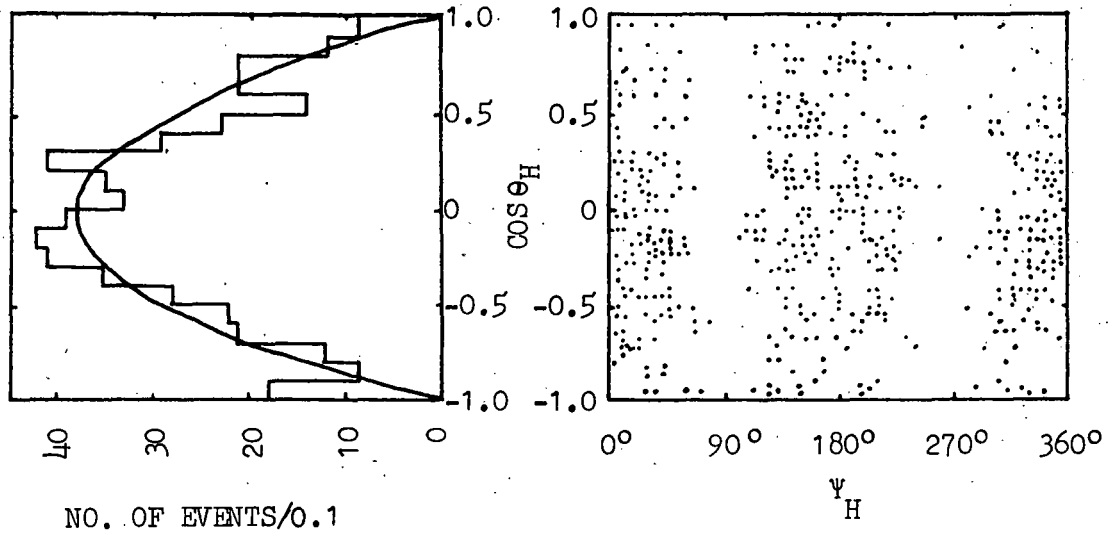

$|t_{min}| \lesssim |t| \lesssim 0.15$ GeV^2

$600 \lesssim M_{2\pi} \lesssim 850$ MeV

505 EVENTS

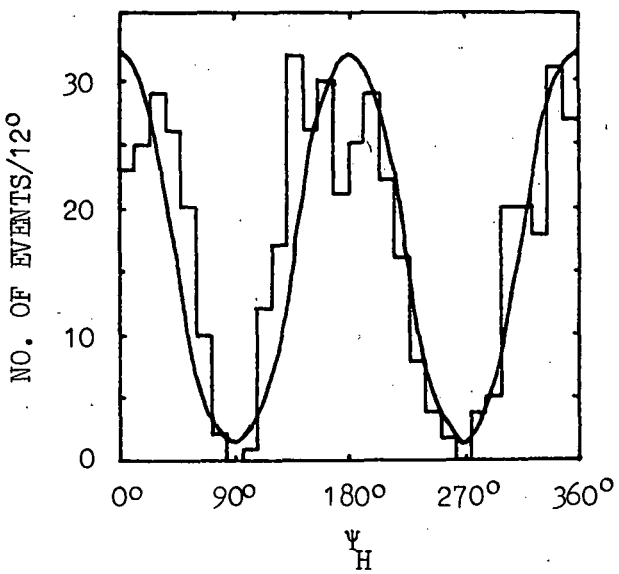

Fig. 10

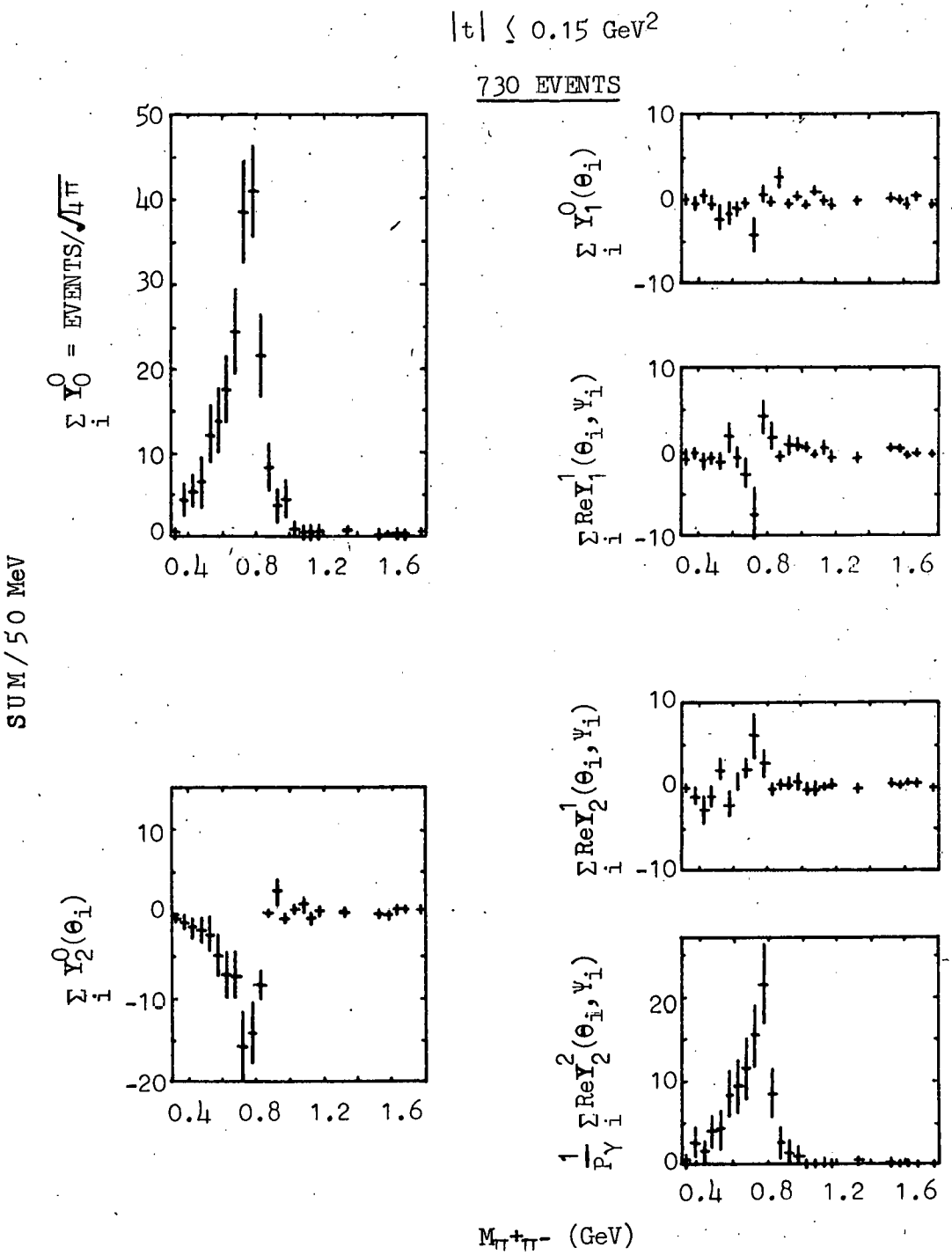
$|t| \lesssim 0.15$ GeV^2
730 EVENTS
SUM / 50 MeV
$\sum_i Y_0^0$ = EVENTS/$\sqrt{4\pi}$
$\sum_i Y_0^0(\theta_i)$
$\sum_i Y_1^0(\theta_i)$
$\sum_i \mathrm{Re}Y_1^1(\theta_i,\Psi_i)$
$\sum_i \mathrm{Re}Y_2^1(\theta_i,\Psi_i)$
$\frac{1}{P_\gamma}\sum_i \mathrm{Re}Y_2^2(\theta_i,\Psi_i)$
$M_{\pi^+\pi^-}$ (GeV)

Fig. 11(a)

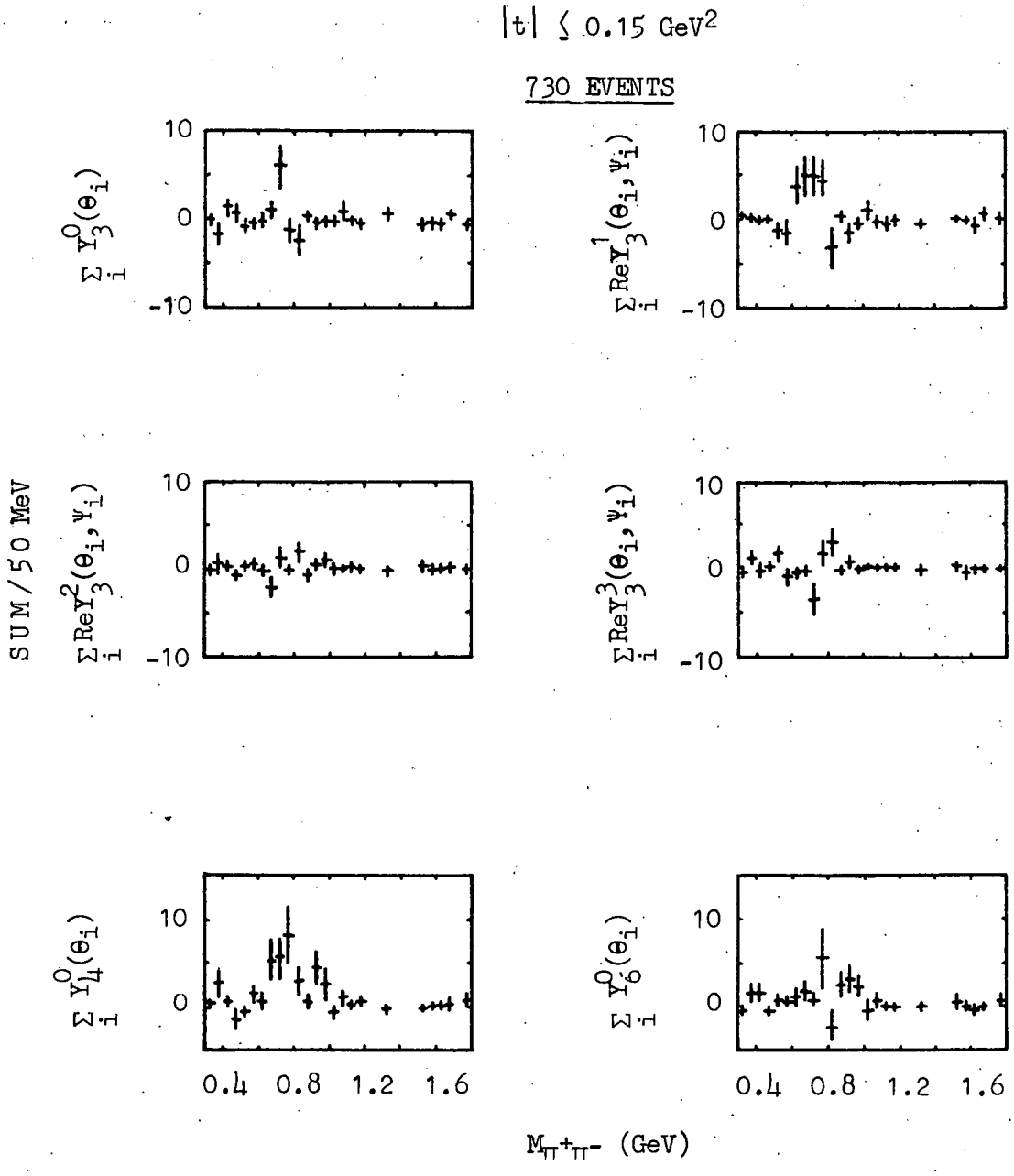
|t| ≲ 0.15 GeV²
730 EVENTS
SUM/50 MeV
$\sum_i Y_3^0(\theta_i)$
$\sum_i \mathrm{Re}Y_3^1(\theta_i,\psi_i)$
$\sum_i \mathrm{Re}Y_3^2(\theta_i,\psi_i)$
$\sum_i \mathrm{Re}Y_3^3(\theta_i,\psi_i)$
$\sum_i Y_4^0(\theta_i)$
$\sum_i Y_6^0(\theta_i)$
10
0
-10
0.4
0.8
1.2
1.6
$M_{\pi^+\pi^-}$ (GeV)

Fig. 11(b)

on deuteron, all $\rho^{\alpha}_{\lambda\lambda'}$ would be zero except

$$\rho^{1}_{1-1} = - \mathrm{Im}\rho^{2}_{1-1} = \frac{1}{2} \qquad \ldots\ldots\ldots (5)$$

Our results for nine independent density matrix elements in Eq. 3, determined by moment analysis[30] (see Appendix B), are given in Table 4 and Fig. 12. Within errors, upto $-t \approx 0.25$ GeV^2, these results clearly show that in helicity frame the contribution from helicity flip are consistent with zero value and ρ^{o} does retain the photon polarization.

For completeness we notice that zero flip in the G-J frame would imply no spin exchange in the t-channel, while zero flip in the Adair frame would hold if spin direction was conserved.[31] Since the matrix elements vary significantly with t in G-J frame, this possibility is ruled out. The most concise way to demonstrate the apparent conservation of helicity in ρ^{o} photoproduction is presented in Fig. 13. Consider a frame in the rest system of the ρ^{o}, in which ρ^{o} density matrix most closely resembles that of the initial photon. Then let β be the angle of rotation around the normal to the production plane, that transforms the s-channel helicity frame into this new frame. One actually minimizes[10]

$$\chi^2(\beta) = \sum_{\lambda,\lambda',\alpha} \left| \frac{\rho^{\alpha}_{\lambda\lambda'}(\beta) - \rho^{\alpha}_{\lambda\lambda'}(\text{Photon})}{\delta\rho^{\alpha}_{\lambda\lambda'}(\beta)} \right|^2$$

where $\rho^{\alpha}_{\lambda\lambda'}$ (Photon) is the ρ^{o} density matrix of photon (Eq. 5).

TABLE 4 (a)

Rho-density matrix elements for the reaction $\gamma d \rightarrow \rho^{o} d$

HELICITY FRAME

$\lvert t \rvert$ GeV^2	t_{min} - 0.02	0.02 - 0.04	0.04 - 0.08	0.08 - 0.12	0.12 - 0.25
ρ^0_{00}	0.138±0.038	0.068±0.058	0.074±0.052	0.128±0.082	0.054±0.082
$Re\rho^0_{10}$	0.036±0.020	-0.033±0.039	-0.048±0.036	0.058±0.056	0.030±0.058
ρ^0_{1-1}	-0.011±0.036	-0.001±0.065	-0.056±0.058	-0.022±0.092	0.155±0.101
ρ^1_{00}	-0.059±0.060	0.070±0.094	-0.166±0.074	0.140±0.149	-0.115±0.108
ρ^1_{11}	0.115±0.046	0.054±0.084	0.068±0.066	-0.086±0.107	-0.016±0.128
$Re\rho^1_{10}$	-0.023±0.030	0.038±0.058	0.030±0.057	0.006±0.085	-0.119±0.094
ρ^1_{1-1}	0.428±0.052	0.454±0.089	0.372±0.076	0.477±0.135	0.395±0.156
$Im\rho^2_{10}$	0.019±0.031	-0.125±0.063	0.040±0.052	0.140±0.079	-0.013±0.090
$Im\rho^2_{1-1}$	-0.399±0.051	-0.478±0.095	-0.449±0.086	-0.521±0.127	-0.273±0.138

TABLE 4 (b)

Rho-density matrix elements for the reaction $\gamma d \to \rho^o d$

GOTTFRIED-JACKSON FRAME

$\lvert t \rvert$ GeV^2	t_{min} - 0.02	0.02 - 0.04	0.04 - 0.08	0.08 - 0.12	0.12 - 0.25
ρ^0_{00}	0.189±0.039	0.129±0.061	0.204±0.057	0.405±0.097	0.316±0.105
$Re\rho^0_{10}$	0.095±0.021	0.110±0.039	0.171±0.033	0.134±0.053	0.077±0.054
ρ^0_{1-1}	0.014±0.035	0.029±0.063	0.009±0.056	0.116±0.083	0.286±0.087
ρ^1_{00}	-0.098±0.060	0.013±0.097	-0.168±0.092	-0.224±0.165	-0.483±0.172
ρ^1_{11}	0.134±0.044	0.082±0.078	0.070±0.067	0.096±0.100	0.168±0.116
$Re\rho^1_{10}$	-0.058±0.063	-0.117±0.063	-0.062±0.047	-0.247±0.081	-0.138±0.078
ρ^1_{1-1}	0.408±0.050	0.426±0.084	0.371±0.078	0.296±0.136	0.211±0.154
$Im\rho^2_{10}$	0.091±0.030	0.056±0.064	0.235±0.056	0.342±0.090	0.174±0.099
$Im\rho^2_{1-1}$	-0.375±0.051	-0.498±0.094	-0.308±0.082	-0.189±0.116	-0.157±0.126

TABLE 4 (c)

Rho-density matrix elements for the reaction $\gamma d \rightarrow \rho^{o} d$

ADAIR FRAME

$\lvert t \rvert$ GeV^2	t_{min} - 0.02	0.02 - 0.04	0.04 - 0.08	0.08 - 0.12	0.12 - 0.25
ρ^0_{00}	0.143±0.038	0.063±0.058	0.063±0.052	0.161±0.084	0.079±0.081
$Re\rho^0_{10}$	0.047±0.020	-0.011±0.039	-0.009±0.035	0.092±0.054	0.071±0.058
ρ^0_{1-1}	-0.009±0.036	-0.004±0.065	-0.061±0.059	-0.006±0.093	0.167±0.101
ρ^1_{00}	-0.063±0.060	0.075±0.095	-0.156±0.073	0.127±0.153	-0.184±0.108
ρ^1_{11}	0.117±0.045	0.051±0.084	0.063±0.067	-0.080±0.106	0.018±0.123
$Re\rho^1_{10}$	-0.030±0.030	0.009±0.057	0.019±0.057	-0.066±0.083	-0.150±0.098
ρ^1_{1-1}	0.426±0.051	0.457±0.088	0.377±0.076	0.471±0.137	0.361±0.155
$Im\rho^2_{10}$	0.030±0.030	-0.097±0.063	0.076±0.052	0.194±0.082	0.025±0.092
$Im\rho^2_{1-1}$	-0.396±0.095	-0.490±0.095	-0.438±0.086	-0.486±0.124	-0.272±0.135

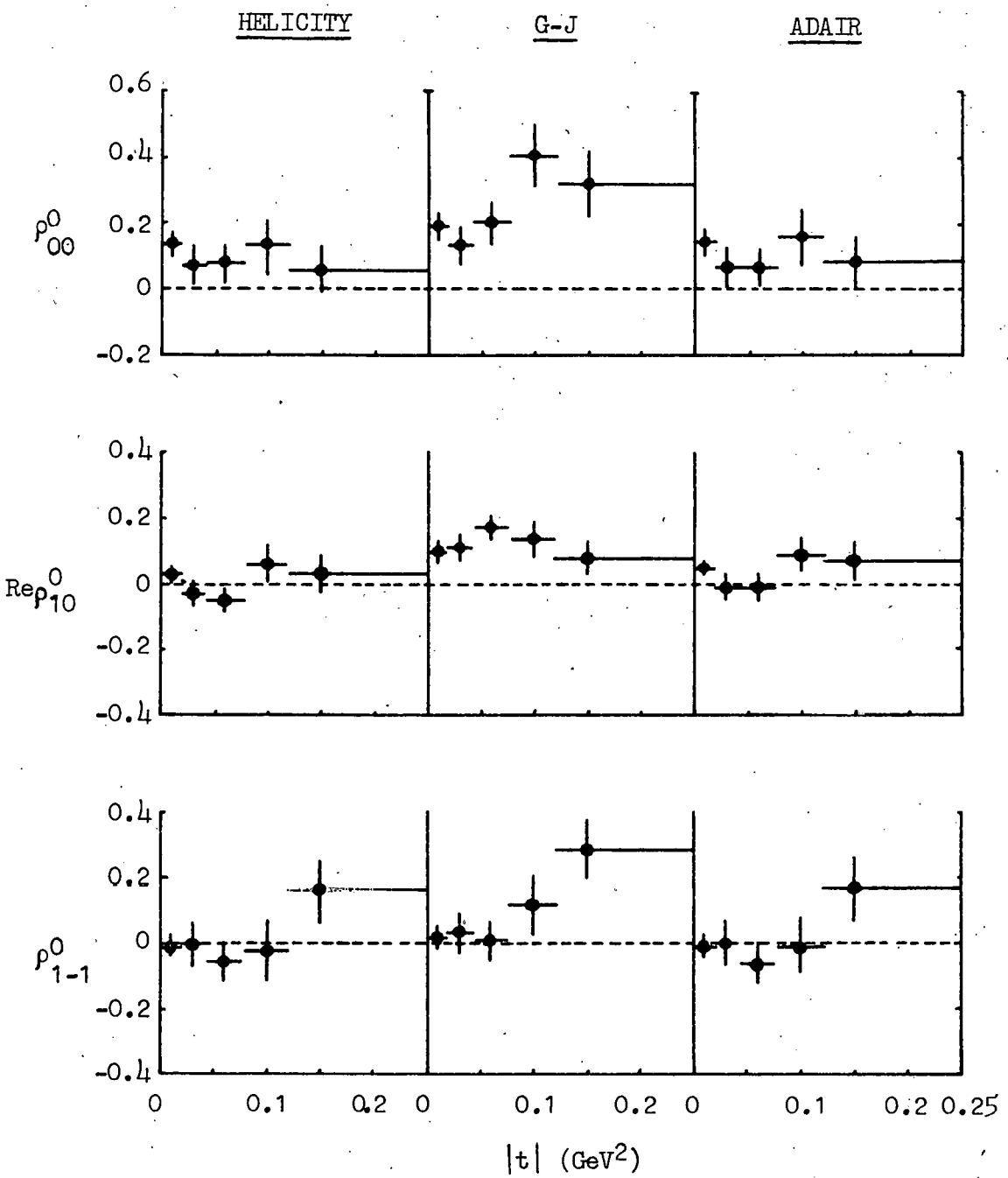
HELICITY
G-J
ADAIR
ρ^0_{00}
$\mathrm{Re}\rho^0_{10}$
ρ^0_{1-1}
0.6
0.4
0.2
0
-0.2
-0.4
0
0.1
0.2
0.25
$|t|$ (GeV^2)

Fig. 12(a)

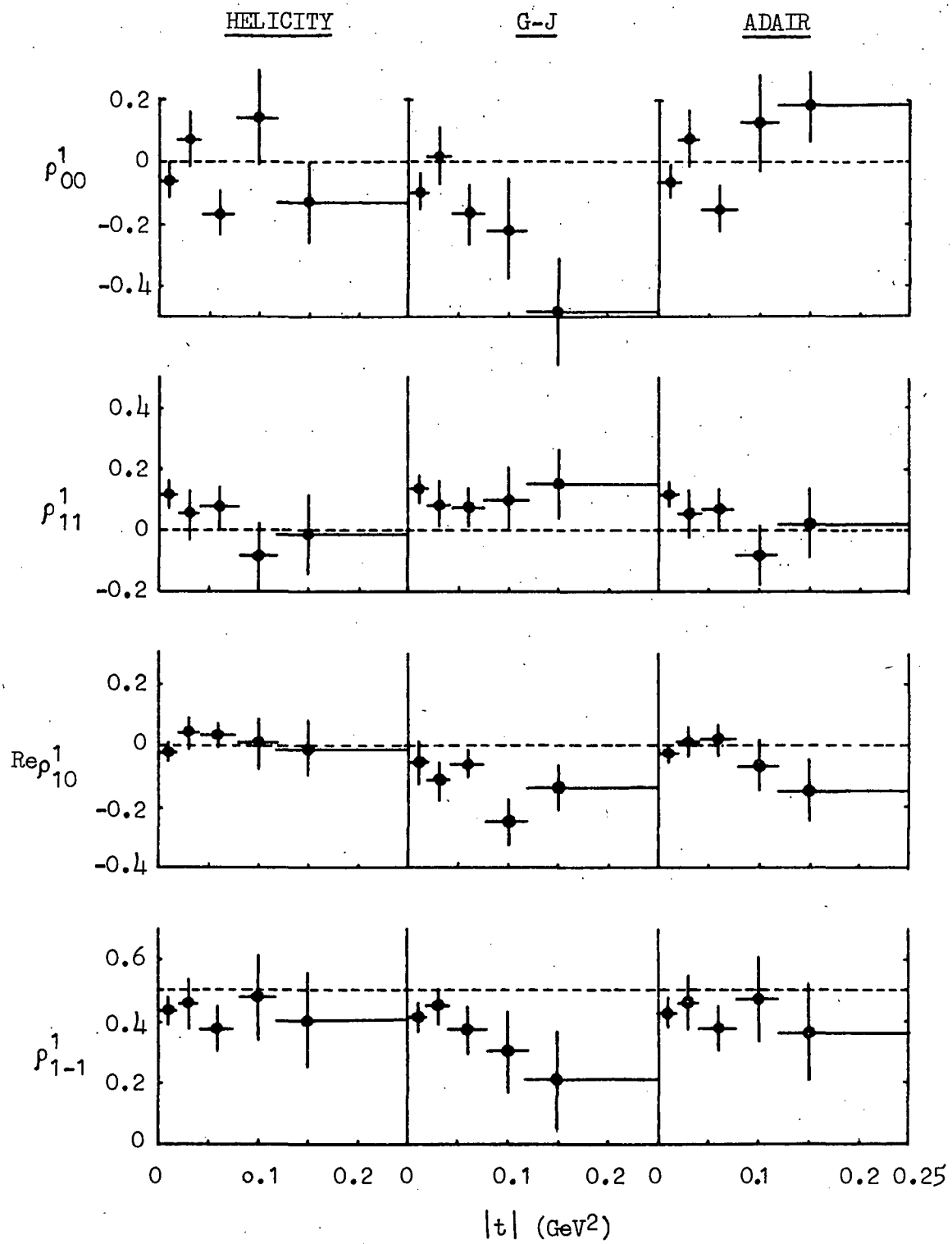
HELICITY
G-J
ADAIR
ρ^1_{00}
ρ^1_{11}
$\mathrm{Re}\rho^1_{10}$
ρ^1_{1-1}
0.2
0
-0.2
-0.4
0.4
0.2
0
-0.2
0.2
0
-0.2
-0.4
0.6
0.4
0.2
0
0
0.1
0.2
0
0.1
0.2
0
0.1
0.2
0.25
$|t|$ (GeV^2)

Fig. 12(b)

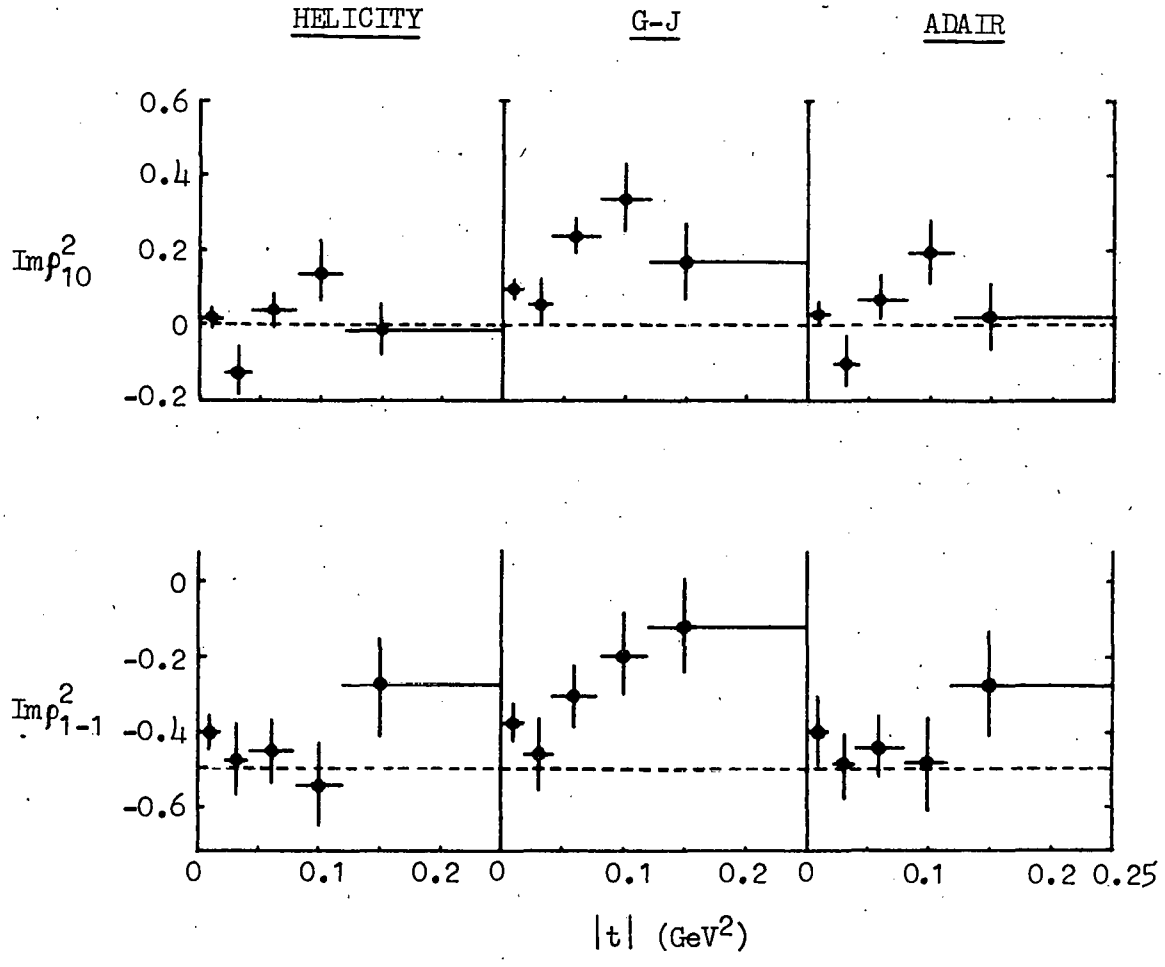
HELICITY
G-J
ADAIR
$\mathrm{Im}\rho^2_{10}$
$\mathrm{Im}\rho^2_{1-1}$
0.6
0.4
0.2
0
-0.2
-0.4
-0.6
0.1
0.25
$|t|$ (GeV^2)

Fig. 12(c)

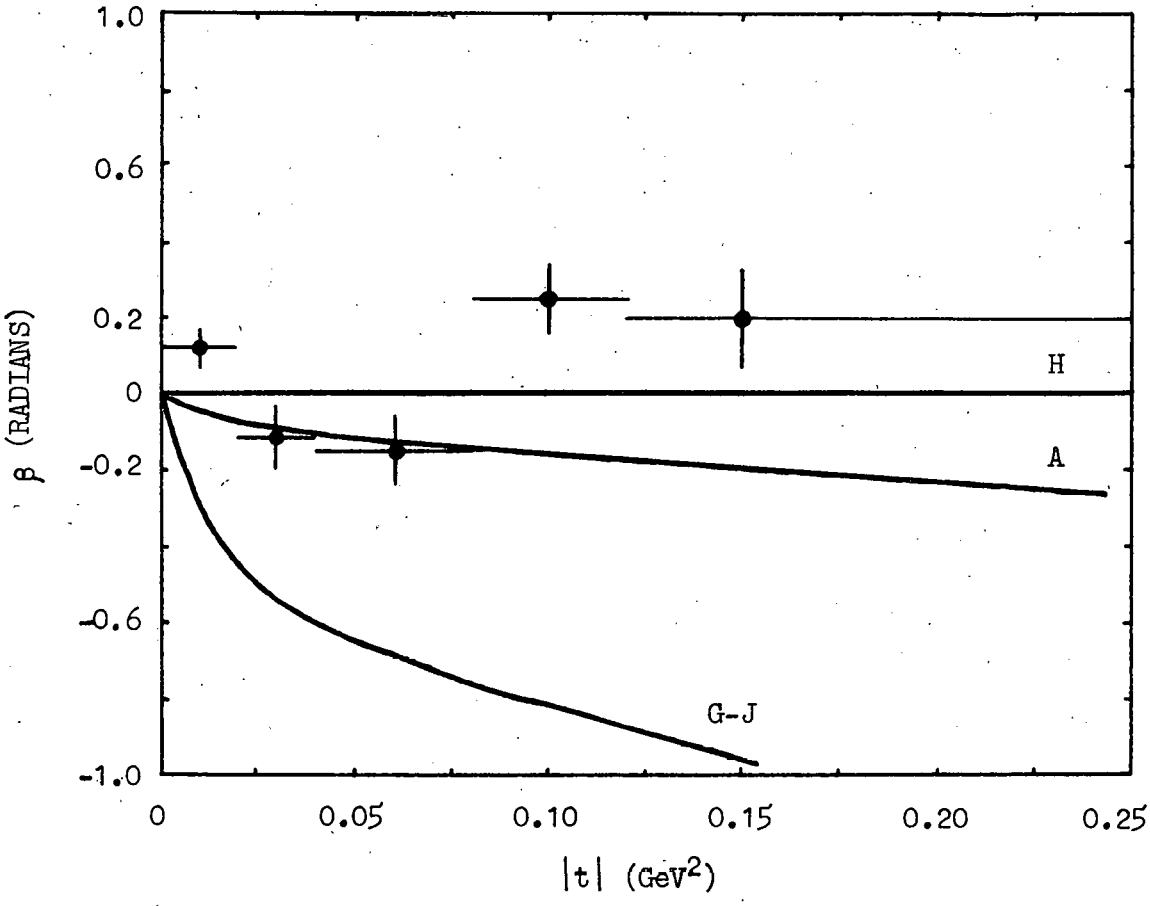

Fig. 13

It is seen in Fig. 13 that β is not far from zero upto $-t = 0.25\ GeV^2$. Also shown in this figure are the angles of rotations from the helicity frame into the Adair frame (curve A), and into the Gottfried-Jackson frame (curve G-J). For $|t| \leq 0.25\ GeV^2$, helicity frame is definitely preferred.

C. Rho Production Properties

It has been shown that to leading order in energy,[32,33] the overall production cross section, σ, may be split into non-interfering contributions σ^N, σ^U from natural and unnatural parity exchanges in the t-channel. One could draw stronger conclusions from the density matrix elements by estimating quantitatively the contributions of σ^N and σ^U to the cross section. The 'parity asymmetry' parameter is defined as

$$P_\sigma = \frac{\sigma^N - \sigma^U}{\sigma^N + \sigma^U}$$

At high energies $P_\sigma = 2\rho^1_{1-1} - \rho^1_{00}$ ..... (7)

Also the 'asymmetry ratio' is given as

$$\Sigma = \frac{\sigma_\parallel - \sigma_\perp}{\sigma_\parallel + \sigma_\perp} = \frac{\rho^1_{11} + \rho^1_{1-1}}{\rho^0_{11} + \rho^0_{1-1}} \quad \ldots (8)$$

where $\sigma_\parallel$ ($\sigma_\perp$) is the cross section for the case when the ρ^0 polarization $\vec{\epsilon}_{\pi+}$ is orthogonal to the production plane and the $\vec{\epsilon}_\gamma$ is parallel (perpendicular) to $\vec{\epsilon}_{\pi+}$.

In Table 5 and Fig. 14 we display the quantities P_σ and

TABLE 5

P_σ and Σ for the reaction $\gamma d \rightarrow \rho^o d$

$\lvert t \rvert$ GeV^2	$P_\sigma = \frac{\sigma^N - \sigma^U}{\sigma^N + \sigma^U}$	$\Sigma = \frac{\sigma_{\parallel} - \sigma_{\perp}}{\sigma_{\parallel} + \sigma_{\perp}}$
t_{min} - 0.02	0.915±0.119	1.293±0.185
0.02 - 0.04	0.838±0.201	1.093±0.286
0.04 - 0.08	0.910±0.168	1.082±0.273
0.08 - 0.12	0.815±0.308	0.947±0.447
0.12 - 0.25	0.905±0.330	0.603±0.328

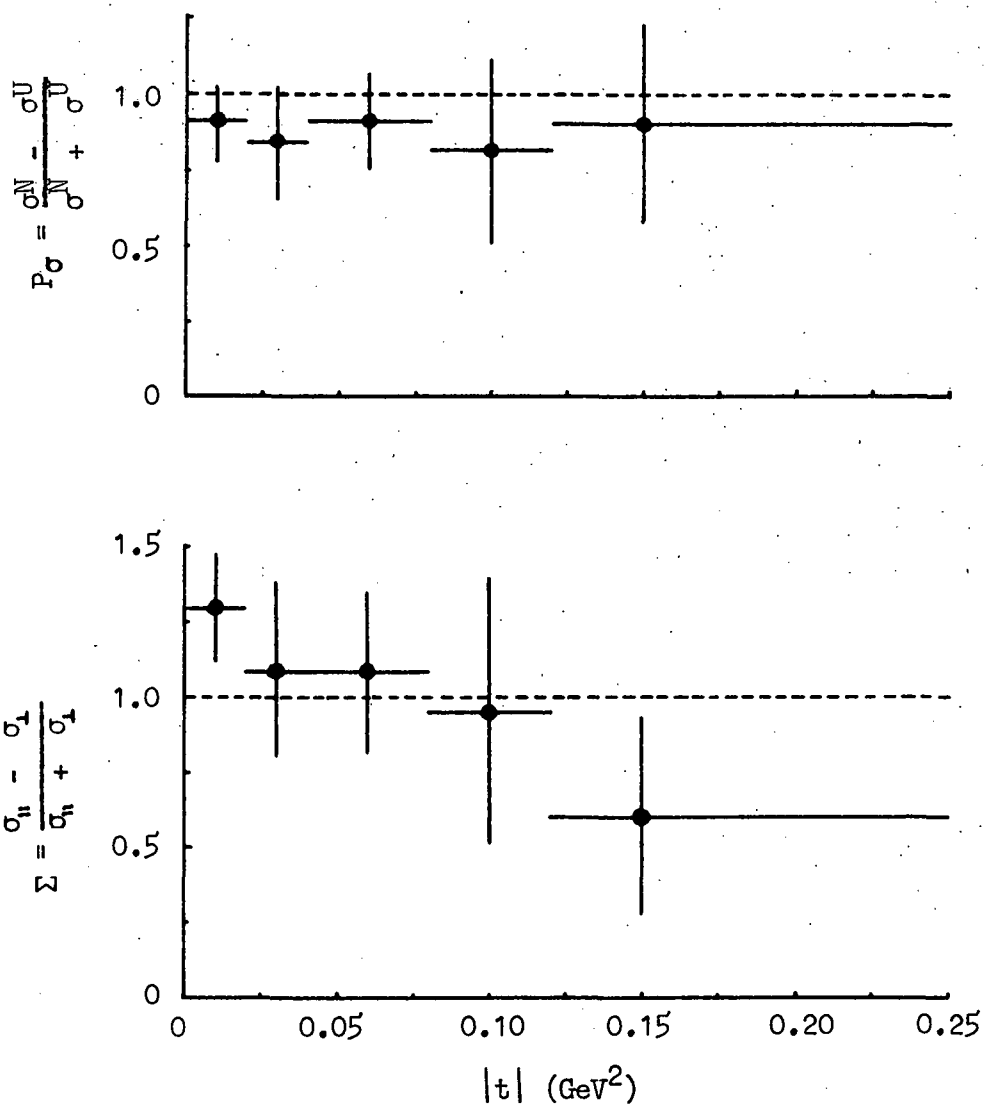
$P_\sigma = \frac{\sigma_N^+ - \sigma_N^-}{\sigma_N^+ + \sigma_N^-}$
1.0
0.5
0
$\Sigma = \frac{\sigma_\parallel - \sigma_\perp}{\sigma_\parallel + \sigma_\perp}$
1.5
1.0
0.5
0
0
0.05
0.10
0.15
0.20
0.25
$|t|$ (GeV^2)

Fig. 14

Σ. We found the contribution from the unnatural parity exchanges to be (5.3 ± 4.5)% and the value of Σ as 1.1 ± 0.2 for the averages over the momentum transfer range of t_{min} - 0.25 GeV^2.

To see whether p-wave $\pi^+\pi^-$ system produced by natural exchanges and with helicity conservation are also seen outside the ρ^o mass region, we have plotted in Fig. 15 ρ^o_{00} and ρ^1_{1-1} in helicity frame, and P_σ as a function of $\pi^+\pi^-$ mass. In the ρ^o mass region

ρ^o_{00} = degree of longitudinal polarization of the $\pi^+\pi^-$ system,
= 0

ρ^1_{1-1} = correlation term between ρ^o helicity (= ±1) states for linearly polarized photons, = 1/2

P_σ = parity asymmetry = 1

but outside of the ρ^o mass region these quantities change drastically. This is clear evidence for a background behaving quite different from the ρ^o.

D. s-Channel Helicity-Conserving p-Wave Intensity

In order to determine directly the amount of p-wave dipion production in the ρ^o mass region, we make use of the result of the section B that the production mechanism for p-wave $\pi^+\pi^-$ pairs conserves s-channel helicity at the $\gamma\pi^+\pi^-$ vertex for $|t| \leq 0.25$ GeV^2, and so yields pion pairs in a well defined spin state. This implies that the decay angular

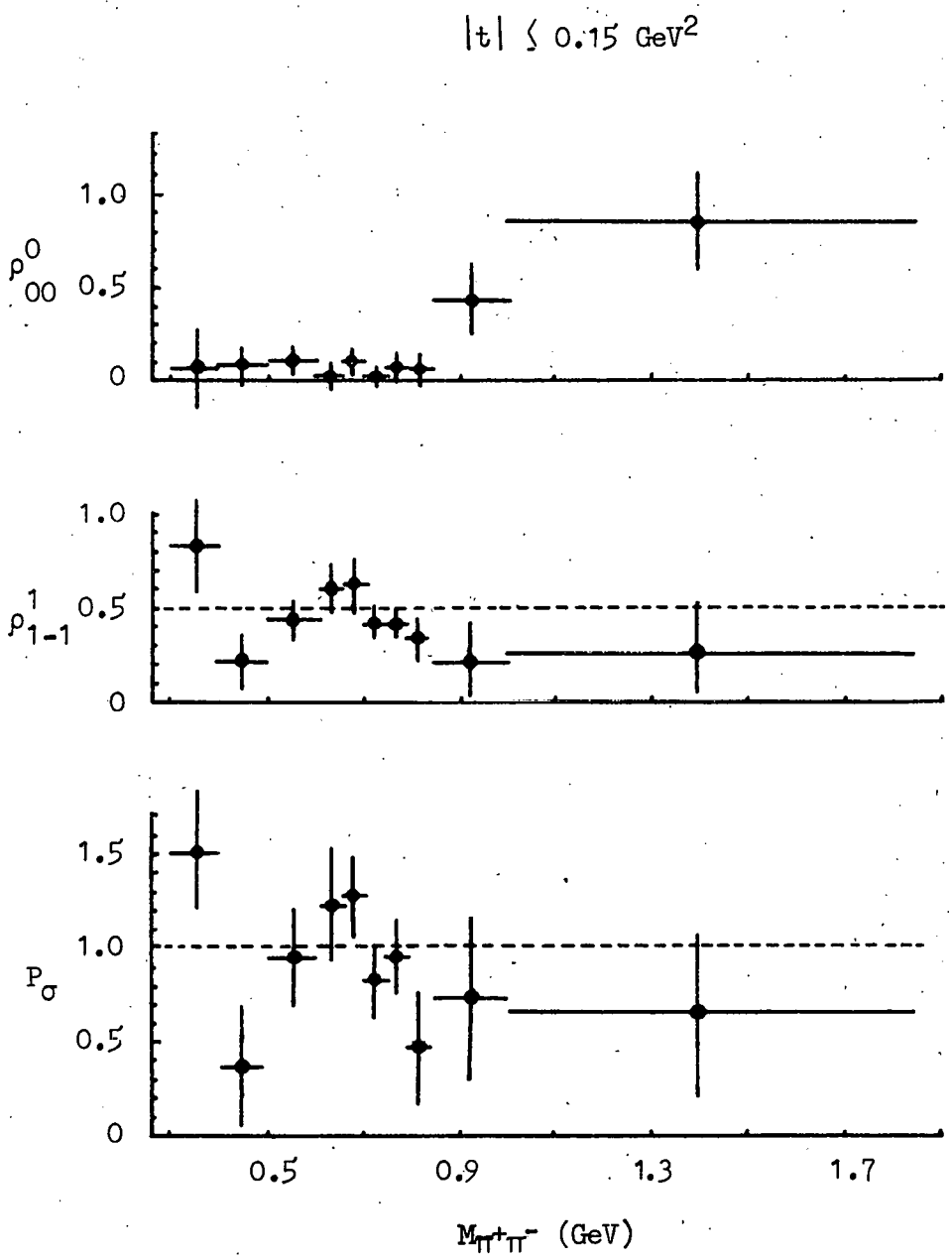
|t| ≤ 0.15 GeV²
1.0
0.5
0
ρ^0_{00}
1.0
0.5
0
ρ^1_{1-1}
1.5
1.0
0.5
0
P_σ
0.5
0.9
1.3
1.7
$M_{\pi^+\pi^-}$ (GeV)

Fig. 15

distribution for p-wave $\pi^+\pi^-$ pairs is given by Eq. 4, which may be expressed in terms of moments as

$$W(\theta,\psi) = \frac{1}{\sqrt{4\pi}} Y_{00}^{o}(\theta) - \frac{1}{\sqrt{20\pi}} Y_2^o(\theta) + 2P_\gamma \sqrt{\frac{3}{40\pi}} \mathrm{Re}Y_2^2(\theta,\psi)$$

In this equation $\mathrm{Re}Y_2^2(\theta,\psi)$ is least affected by background due to its ψ dependence and used, therefore, to determine the s-channel c.m.s. helicity-conserving p-wave $\pi^+\pi^-$ intensity, I_p, defined as[10]

$$I_p = \frac{\sum_i \mathrm{Re}Y_2^2(\theta_i,\psi_i)}{\langle \mathrm{Re}Y_2^2(\theta_i,\psi_i)\rangle}$$

$$= \frac{\sum_i \mathrm{Re}Y_2^2(\theta_i,\psi_i)}{\iint d\psi\, d(\cos\theta)\cdot W(\theta,\psi)\cdot \mathrm{Re}Y_2^2(\theta,\psi)}$$

After carrying out the integration, we get

$$I_p = \frac{1}{P_\gamma}\sqrt{\frac{40\pi}{3}} \sum_i \mathrm{Re}Y_2^2(\theta_i,\psi_i)$$

$$I_p = \frac{2.5}{P_\gamma} \sum_i \sin^2\theta_i \cdot \cos 2\psi_i \qquad \ldots\ldots\ldots (9)$$

Here the summation is over all events. Figure 16 shows the distribution of I_p as a function of t. For $-t \approx 0.1$ GeV^2, the slope of t-distribution and the slope obtained for I_p agree within errors.

In Fig. 5 the dots marked on the histograms show the I_p as a function of $\pi^+\pi^-$ for different t-intervals. We notice

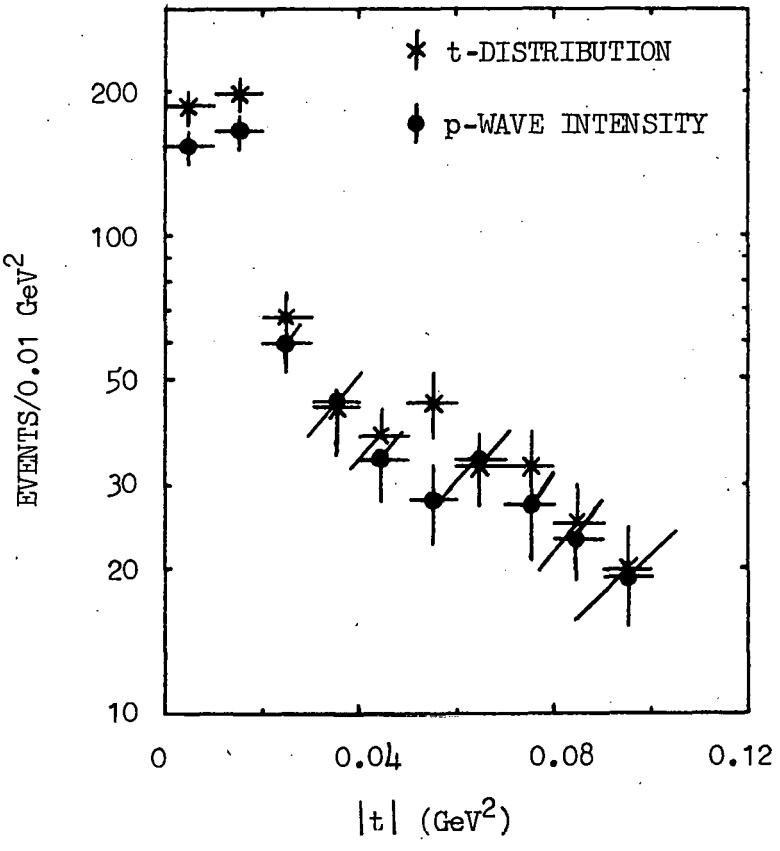
t-DISTRIBUTION
p-WAVE INTENSITY
200
100
50
30
20
10
EVENTS/0.01 GeV^2
0
0.04
0.08
0.12
|t| (GeV^2)

Fig. 16

that the I_p accounts for almost all the events within errors and shows the same skewing (characteristic downward ρ mass shift in photoproduction) as the mass distributions.

V. CROSS SECTION DETERMINATION

The electron pairs, although principal background, provide a means to calculate cross section with very little bias. The photoproduction cross section for hadronic events is obtained by relating the number of hadronic events, N_H, to the number of e^+e^- pairs, N_P, obtained in the same scanning volume (see Chapter II B), using the known[34] cross section, σ_P, for e^+e^- pair production:

$$\sigma_H = \frac{N_H}{N_P} \cdot \sigma_P \qquad \ldots\ldots\ldots (10)$$

Corrections for scanning losses were applied. The losses of two-prong events were mainly due to high intensity of the e^+e^- pair background, and due to events having very small projected opening angles and could not be distinguished from the e^+e^- pairs.

A. Pair Production Cross Section

Knasel[34] evaluated, numerically precise to ± 0.5%, the e^+e^- pair production cross section, after applying various corrections to the theoretical results of Jost, Luttinger, and Slotnick.[35] Knasel used the work of Mork[36] and Mork and Olsen[37] to account for retardation effect and radiative corrections. The experimental work at DESY[38] has obtained values for the total cross sections for pair production in hydrogen and deuterium (which should have the same value as

hydrogen except for possible differences in the molecular wave function of deuterium). Table 6 shows a comparison of these numbers, with the calculated values of Knasel. In general the hydrogen and deuterium data are same within statistical errors, showing that the molecular correction differences between the two different states are not observed. Although the data gave on the average 1% larger cross sections as compared with the theoretical values, one must regard a good agreement between experiment and theory as the difference is only about one standard deviation. Moreover, refinement of the DESY measurements could in principle allow a 0.1 percent absolute measurement.[39] From Knasel's data we have used an average value of 20.1 ± 0.1 mb for the total pair production cross section over the photon energy range of 4.7 - 6.2 GeV.

B. Differential Cross Section for $\gamma d \longrightarrow \rho^{o} d$

To the reaction $\gamma d \longrightarrow \pi^{+}\pi^{-} d$ a total of 1176 two and three prong events fitted within fitted photon energy range of 4.7 - 6.2 GeV. To calculate the total cross section for ρ^{o} production in this channel, we made the following three corrections:

1. Correction for Scanning

a) Due to small opening angles in projection:

We have applied the scanning correction for those events which has very small projected opening angle and could

TABLE 6

Total pair production cross sections
in hydrogen and deuterium

Photon Energy GeV	Theory σ_T mb	Hydrogen σ_T mb	Deuterium σ_T mb	Average of H_2 and D_2
0.55	17.1	15.54±0.5		15.54±0.5
0.87	18.0	17.52±0.8		17.52±0.8
1.18	18.6	18.63±0.9		18.63±0.9
1.46	18.9	18.91±0.20	18.89±0.18	18.90±0.14
1.98	19.2	19.06±0.33	19.70±0.23	19.38±0.20
2.55	19.5	19.61±0.28	19.62±0.26	19.62±0.20
2.99	19.7	19.57±0.30	20.00±0.19	20.08±0.20
3.46	19.8	19.70±0.24	19.97±0.23	19.84±0.17
3.98	19.9	20.02±0.30	20.49±0.21	20.26±0.20
4.55	19.9	20.19±0.33	20.34±0.25	20.27±0.20
4.99	20.0	19.58±0.18	20.28±0.15	19.93±0.10
5.46	20.1	19.90±0.25	20.25±0.15	20.07±0.15
5.98	20.1	20.17±0.21	20.34±0.20	20.25±0.15
6.55	20.2	20.50±0.24	20.76±0.18	20.63±0.15

not be distinguished from e^+e^- pairs. Losses due to this were estimated by determining the deviation from the isotropy in the distribution of the angle between the optical axis direction and the projection of the vector ($\vec{\pi}^+ \times \vec{\pi}^-$) onto the plane perpendicular to the beam direction. In the laboratory frame $\vec{\pi}$ is the three-momentum of pion. The estimated correction was (33 ± 5)% for this reaction.

b) Due to high e^+e^- pair background

Losses due to high intensity of the e^+e^- pair background were estimeted from the double-scan efficiencies of two and three prong events (Chapter II B). This gave a correction of (8 ± 1)% to the events.

2. Correction for Unprocessed Events

The unprocessed events consists of those events which are unmeasurable, poorly measured, and no fit events (Table 2). We have distributed among the different channels these two and three prong events in the same proportions as the fitted events. In case of ambiguity between a 3C and 0C fits, the 3C was given a weighting factor of one. Whereas for n ambiguities amongst 3C fits the weighting factor was 1/n for each channel. This distribution gave a total correction of (11 ± 1)% to the events.

3. Correction for Photon Energy Selection

The e^+e^- pairs have been counted (Chapter II B) without imposing any selection criteria on the incoming photon energy. But the hadronic events are considered only within

the fitted photon energy range of 4.7 - 6.2 GeV. To correct for the difference between the energy spectra of the pairs counted and that of ρ^o events, we have used the photon energy spectra of Fig. 3. This correction was (18 ± 3) percent.

After putting in all these corrections the total ρ^o photoproduction cross section in this channel comes out to be (9.1 ± 0.8) μb. The error also includes uncertainty due to the background. This is in good agreement with the previously obtained values.[12]

C. Photoproduction of Other Mesons

To investigate the production of ω, ϕ, ρ', and A_1 mesons in the final states $\pi^+\pi^-\pi^o d$, $K^+K^- d$, $2\pi^+2\pi^- d$, and $\pi^+2\pi^- pp$, respectively, the following reactions were looked into:

$$\gamma d \longrightarrow \pi^+\pi^-\pi^o d \quad \ldots\ldots\ldots (11)$$

$$\gamma d \longrightarrow K^+K^- d \quad \ldots\ldots\ldots (12)$$

$$\gamma d \longrightarrow 2\pi^+2\pi^- d \quad \ldots\ldots\ldots (13)$$

$$\gamma d \longrightarrow \pi^+2\pi^- pp \quad \ldots\ldots\ldots (14)$$

For further studies only those events were considered which had fitted photon energy in the interval 4.7 - 6.2 GeV. No attempts were made to resolve the fit ambiguities of these channels with the other channels (Table 2).

a) Photoproduction of ω and ϕ mesons

There are not as many experiments on coherent ω and ϕ photoproduction as for ρ^o. These experiments are more

difficult in that we are dealing with a much smaller cross-sections, and the decay modes are more difficult to isolate. The only bubble chamber data at 4.3 GeV on coherent ϕ photoproduction, $\gamma d \rightarrow \phi d$, have been published by Weizmann group[12] (1972) with rather large statistical uncertainties. The meson photoproduction on d at 6.2 and 8.25 GeV has been studied only at Cornell[40] using counters.

We attempted both the hypotheses (11) and (12) for the three-prong events. For the two-prong events hypothesis (11) was not tried, because in this reaction the events with invisible d recoil have two unmeasured particles which are difficult to handle. The 3π and 2K mass distributions for the reactions (11) and (12), respectively, in Fig. 17 are for $-t < 0.15$ GeV^2 (momentum transfer from the target to the recoil deuteron). There are indications of ω and ϕ productions in these mass distributions, but the statistics is insufficient to make mass fits.

b) Photoproduction of ρ' meson

There are several reasons to expect vector mesons heavier than the ϕ to exist. The existence of such particles would have a great impact on the vector dominance model. It is of general interest, beyond the VDM, to search for such particles since the quark model and Veneziano model predict the existence of states at masses of ~1.25 GeV and between 1.5 - 1.6 GeV. Coherent photoproduction of such a meson, ρ', has been reported by Smadja *et al.*[41] from the reaction

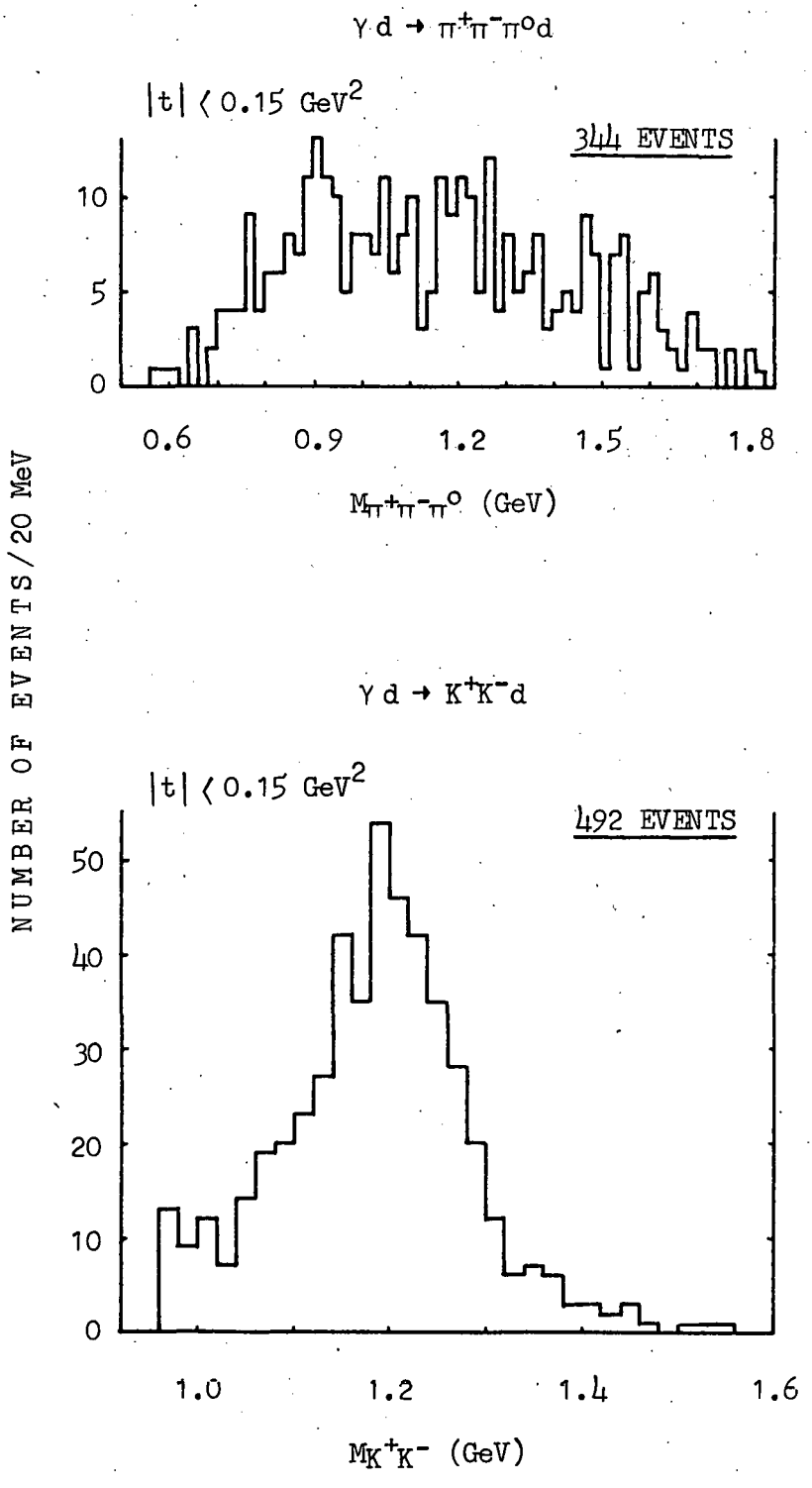
γ d → π⁺π⁻π°d
|t| < 0.15 GeV²
344 EVENTS
10
5
0
0.6
0.9
1.2
1.5
1.8
Mπ⁺π⁻π° (GeV)
γ d → K⁺K⁻d
|t| < 0.15 GeV²
492 EVENTS
50
40
30
20
10
0
1.0
1.2
1.4
1.6
MK⁺K⁻ (GeV)
NUMBER OF EVENTS / 20 MeV

Fig. 17

$\gamma p \rightarrow p 2\pi^+ 2\pi^-$ at 9.3 GeV. The 4π mass spectrum showed an enhancement near 1.6 GeV.

All the four and five prong events were attempted for the hypothesis (13). The 4π mass distribution is shown in Fig. 18. Due to the limited statistics we cannot draw any conclusion with respect to the existence of ρ' meson.

c) Photoproduction of A_1 meson

About using pion beams in studying A_1 meson, a $\rho\pi$ enhancement at 1.1 GeV, it was pointed out[42] that this could also be due to a Deck-type kinematic effect. One of the main reasons to perform our experiment was to study the channel $\gamma n \rightarrow \pi^+\pi^-\pi^- p$. It was suggested by Poe et al.[43] that in this channel the A_1 production would be free from the Deck-effect.

We have tried all the four and five prong events for the hypothesis (14). The 3π mass distribution in Fig. 18 is for $-t < 0.15$ GeV^2, and only those events are plotted here for which at least one of the $\pi^+\pi^-$ mass combinations lies within the mass range of 0.6 - 0.85 GeV. In this mass distribution A_2 peak is present, but there is no indication of A_1 meson production.

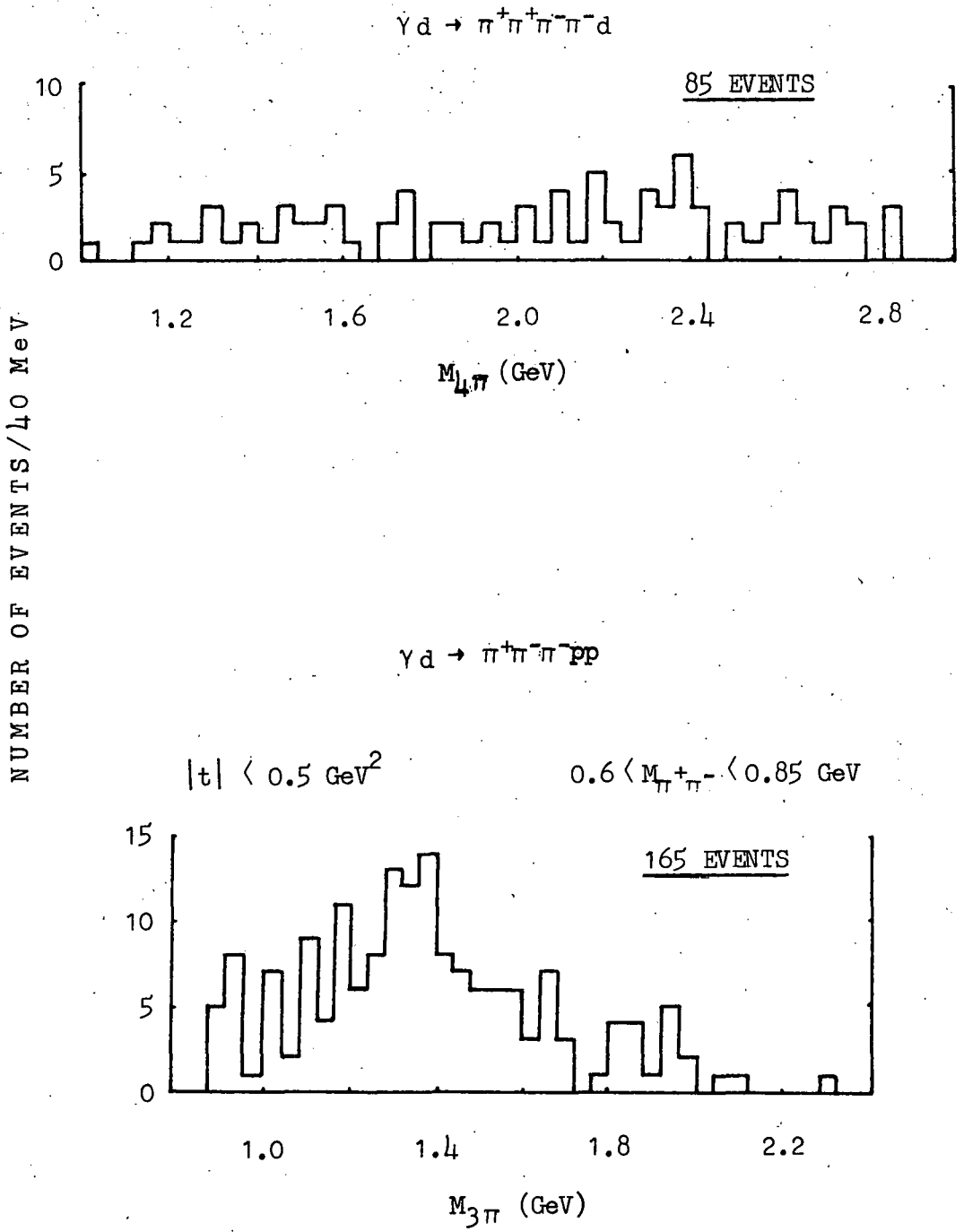
γd → π⁺π⁺π⁻π⁻d
85 EVENTS
10
5
0
1.2
1.6
2.0
2.4
2.8
M4π (GeV)
NUMBER OF EVENTS/40 MeV
γd → π⁺π⁻π⁻pp
|t| < 0.5 GeV²
0.6 < Mπ⁺π⁻ < 0.85 GeV
165 EVENTS
15
10
5
0
1.0
1.4
1.8
2.2
M3π (GeV)

Fig. 18

VI. RESULTS AND CONCLUSIONS

We have found that the ρ^o production in $\gamma d \rightarrow \rho^o d$ channel is shifted to lower masses than found in interactions using pion beams. We have also found that the ρ^o shape is skewed with respect to a p-wave Breit-Wigner distribution, and changes shape as a function of t. The prediction of Ross-Stodolsky that the mass-skewing factor, $(M/M_{\pi\pi})^4$, should work at $t = 0$ is not supported by the data near $t = 0$.

We have been able to determine nine independent ρ^o density matrix elements, because of the high degree of linear polarization of our photon beam. These parameters are given in Table 4 and Fig. 12 for helicity, Gottfried-Jackson, and Adair frames. From these matrix elements we have been able to separate the contributions for ρ^o production by natural and unnatural parity exchanges. It has been found that this reaction proceeds almost completely through the natural parity exchange: the contributions from the unnatural parity exchanges being only $(5.3 \pm 4.5)\%$, and the value of asymmetry ratio, Σ, is 1.1 ± 0.2 over the momentum transfer range of $|t| \leq 0.25$ GeV^2.

The production of the ρ^o in this reaction has been found to conserve s-channel helicity up to $-t \approx 0.15$ GeV^2. We believe that these features may be general characteristics of diffractive processes.[44]

From the parameterized fitting to the data we find the

ρ^{o} mass and width as (766 ± 5) and (139 ± 11) MeV, respectively. The ρ^{o} production cross section in this reaction channel at 5.5 GeV have been found to be (9.1 ± 0.8) μb.

APPENDIX A

Formalism for Analysing Decay of ρ^o Produced by Linearly Polarized Photons

The analysis used the formalism of Schilling *et al.*,[29] as originated by Thews.[28]

If θ and ϕ are the polar and azimuthal angles of the π^+ in the ρ^o rest frame in any coordinate system, the decay angular distribution for ρ^o can be written in terms of its density matrix elements as

$$\frac{dN}{d\phi d(\cos\theta)} = W^o(\cos\theta,\phi) = \frac{3}{4\pi}\left[\frac{1}{2}(1-\rho_{00}) + \frac{1}{2}(3\rho_{00}-1)\cos^2\theta - \sqrt{2}\mathrm{Re}\rho_{10}\sin 2\theta\cos\phi - \rho_{1-1}\sin^2\theta\cos 2\phi\right]$$

If Φ is the angle between the photon electric vector and the production plane (is the same in the total c.m. system and ρ^o rest frame), the density matrix of a real photon of helicity ± 1 with linear polarization P_γ $(0 \leq P_\gamma \leq 1)$ can be written as[29]

$$\rho(\gamma) = \frac{1}{2}\begin{pmatrix} 1 & -P_\gamma e^{-2i\Phi} \\ -P_\gamma e^{2i\Phi} & 1 \end{pmatrix}$$

This can be rewritten in terms of a 2 x 2 unit matrix, I, and three Pauli spinors, σ_i, as

$$\rho(\gamma) = \frac{1}{2}\ (I + \vec{P}_\gamma \cdot \vec{\sigma})$$

where

$$\vec{P}_\gamma = P_\gamma(-\cos 2\Phi, -\sin 2\Phi, 0)$$

The density matrix for the ρ^o, $\rho(v)$, can similarly be written as

$$\rho(v) = \rho^o(v) - P_\gamma[\rho^1(v)\ \cos 2\Phi + \rho^2(v)\ \sin 2\Phi]$$

The matrix $\rho^o(v)$ describes the ρ^o decay in the case of unpolarized beam, whereas, $\rho^1(v)$ and $\rho^2(v)$ occur due to the linear polarization of the photons. The three hermitian matrices $\rho^\alpha(v)$, $\alpha = 0, 1, 2$ read as

$$\rho^o_{mn}(v) = \frac{1}{N} \sum_{\lambda=\pm 1} T_{m\lambda}\ T^\dagger_{n\lambda}$$

$$\rho^1_{mn}(v) = \frac{1}{N} \sum_{\lambda,\lambda'} T_{m\lambda}\ \sigma^1_{\lambda\lambda'}\ T^\dagger_{n\lambda'}$$

$$\rho^2_{mn}(v) = \frac{1}{N} \sum_{\lambda,\lambda'} T_{m\lambda}\ \sigma^2_{\lambda\lambda'}\ T^\dagger_{n\lambda'}$$

The normalization is such that $N = \sum_{m,\lambda} |T_{m\lambda}|^2$. Here T is the usual ρ^o helicity-production amplitude. For convenience we have suppressed the helicities of the target which are also summed in the definition of the density matrix.

The symmetry properties of the helicity amplitudes imply symmetry relations for $\rho(v)$; if Y-axis is taken as the production normal and if the parity is conserved, we get

$$\rho^{\alpha}_{\lambda\lambda'}(v) = (-1)^{\lambda-\lambda'}\ \rho^{\alpha}_{-\lambda-\lambda'}(v) \text{ for } \alpha = 0,1$$

$$\rho^{2}_{\lambda\lambda'}(v) = -\ (-1)^{\lambda-\lambda'}\ \rho^{2}_{-\lambda-\lambda'}(v)$$

The ρ^{o} decay angular distribution can then be expressed in terms of nine independent measurable spin density matrix parameters, ρ^{α}_{mn}, as

$$W(\cos\theta,\phi,\Phi) = W^{o}(\cos\theta,\phi) + P_{\gamma}[\cos 2\Phi W^{1}(\cos\theta,\phi) + \sin 2\Phi W^{2}(\cos\theta,\phi)]$$

where

$$W^{o}(\cos\theta,\phi)=\frac{3}{4\pi}[\frac{1}{2}(1-\rho^{o}_{00}) + \frac{1}{2}(3\rho^{o}_{00}-1)\cos^{2}\theta-\sqrt{2}\mathrm{Re}\rho^{o}_{10}\sin 2\theta\cos\phi - \rho^{o}_{1-1}\sin^{2}\theta\cos 2\phi]$$

$$W^{1}(\cos\theta,\phi)=\frac{3}{4\pi}[\rho^{1}_{11}\sin^{2}\theta + \rho^{1}_{00}\cos^{2}\theta - \sqrt{2}\mathrm{Re}\rho^{1}_{10}\sin 2\theta\cos\phi - \rho^{1}_{1-1}\sin^{2}\theta\cos 2\phi]$$

$$W^{2}(\cos\theta,\phi)=\frac{3}{4\pi}[\sqrt{2}\ \mathrm{Im}\rho^{2}_{10}\sin 2\theta\sin\phi + \mathrm{Im}\rho^{2}_{1-1}\sin^{2}\theta\sin 2\phi]$$

APPENDIX B

Determination of Density Matrix Elements $\rho^{\alpha}_{\lambda\lambda'}$

To determine the nine independent density matrix elements, $\rho^{\alpha}_{\lambda\lambda'}$, we use the method of moments as suggested by Schmitz.[30] The normalized expected value of a function $f(\theta,\phi,\Phi)$ is defined as

$$\langle f(\theta,\phi,\Phi)\rangle = \frac{\int_0^{2\pi}\int_0^{2\pi}\int_{-1}^{+1} d\Phi d\phi d(\cos\theta)\frac{1}{2\pi} \cdot f(\theta,\phi,\Phi) \cdot W(\cos\theta,\phi,\Phi)}{\int_0^{2\pi}\int_0^{2\pi}\int_{-1}^{+1} d\Phi d\phi d(\cos\theta)\frac{1}{2\pi} \cdot W(\cos\theta,\phi,\Phi)}$$

where θ,ϕ,Φ and W are defined in the text. With this definition and the Eq. 3 we get the values of the density matrix elements which are as follows:

$$\rho^{o}_{00} = 2.5\,\langle\cos^2\theta\rangle - 0.5$$

$$\mathrm{Re}\rho_{10} = -1.25\,\langle\sin 2\theta\cos\phi\rangle/\sqrt{2}$$

$$\rho^{o}_{1-1} = -1.25\,\langle\sin^2\theta\cos 2\phi\rangle$$

$$\rho^{1}_{00} = \frac{1}{P_\gamma}\,(\langle\cos 2\Phi\rangle - 5\,\langle\cos^2\theta\,\cos 2\Phi\rangle)$$

$$\rho^{1}_{11} = \frac{1}{P_\gamma}\,(2.5\langle\cos^2\theta\cos 2\Phi\rangle - 1.5\,\langle\cos 2\Phi\rangle)$$

$$\mathrm{Re}\rho^{1}_{10} = \frac{1}{P_\gamma}\,2.5\langle\sin 2\theta\cos\phi\cos 2\Phi\rangle/\sqrt{2}$$

$$\rho^{1}_{1-1} = \frac{1}{P_\gamma}\,2.5\,\langle\sin^2\theta\cos 2\phi\cos 2\Phi\rangle$$

$$\mathrm{Im}\rho^{2}_{10} = -\frac{1}{P_\gamma}\,2.5\langle\sin 2\theta\sin\phi\sin 2\Phi\rangle/\sqrt{2}$$

$$\mathrm{Im}\rho^{2}_{1-1} = -\frac{1}{P_\gamma}\,2.5\langle\sin^2\theta\sin 2\phi\sin 2\Phi\rangle$$

REFERENCES

1. J.J. Sakurai, Ann. Phys. 11, 1 (1960).

2. M. Gell-Mann and F. Zachariasen, Phys. Rev. 124, 953 (1961);

   M. Gell-Mann, Phys. Rev. 125, 1067 (1962);

   N.M. Kroll et al., Phys. Rev. 157, 1376 (1967).

3. Cambridge Bubble Chamber Group, Phys. Rev. 146, 994 (1966).

4. ABBHHM Collaboration, Phys. Rev. 175, 1669 (1968).

5. A. Silverman, Proc. of the 4th Int. Symposium on Electron and Photon Interactions at High Energies, Liverpool 1969 (DNPL, 1969) pp. 71 and Ref. cited there.

6. R. Anderson et al., Phys. Rev. D1, 27 (1970).

7. D. McLeod et al., Phys. Rev. Lett. 7, 383 (1961).

8. L. Criegee et al., Phys. Lett. 28B, 282 (1968), and Phys. Rev. Lett. 25, 1306 (1970).

9. G. Diambrini-Palazzi et al., Phys. Rev. Lett. 25, 478 (1970).

10. SLAC-Berkeley-Tufts Collaboration, Phys. Rev. Lett. 24, 960, 1469 (1970);

    K.C. Moffeit, LBL Report No. UCRL-19890 (Ph.D. Thesis, 1970), unpublished.

11. Y. Eisenberg et al., Phys. Rev. Lett. 25, 764 (1970);

    Y. Eisenberg et al., Nucl. Phys. B42, 349 (1972).

12. H.G. Hilpert et al., Nucl. Phys. B21, 93 (1970), and B23, 45 (1970);

    G. Alexander et al., Nucl. Phys. B68, 1 (1974).

13. J.J. Murray and P.R. Klein, SLAC Report No. TN-67-19 (1967), unpublished.

14. C.K. Sinclair et al., IEEE Trans. on Nucl. Sci. 16, 1065 (1969).

15. R.A. Gearhart et al., Nucl. Instr. and Methods 75, 220 (1969).

16. R.H. Milburn, Phys. Rev. Lett. 10, 75 (1963).

17. F.R. Arutyunian and V.A. Tumanian, Phys. Lett. 4, 176 (1963);

F.R. Arutyunian et al., JETP 18, 218 (1964).

18. W.J. Podolsky, LBL Report No. UCRL-20128 (Ph.D. Thesis, 1971), unpublished.

19. H.C. Albrecht et al., LBL Report No. UCRL-18528 Rev. (1968), unpublished.

20. L.J. Lanzerotti et al., Phys. Rev. 166, 1365 (1968).

21. H.H. Bingham et al., Phys. Rev. Lett. 24, 955 (1970);

J. Ballam et al., Phys. Rev. Lett. 24, 960 (1970).

22. R. Vanderhagen et al., Nucl. Phys. B13, 329 (1969).

23. B. Werner et al., Phys. Rev. 188, 2023 (1969).

24. J.D. Jackson, Nuovo Cim. 34, 1644 (1964).

25. M. Ross and L. Stodolsky, Phys. Rev. 149, 1172 (1966).

26. P.H. Eberhard and W.O. Koellner, Computer Phys. Commun. 3, 296 (1972), and 5, 163 (1973).

27. J. Friedman, SAGE, Group A Programming Note-P-189 (1969), LBL, unpublished.

28. R.L. Thews, Phys. Rev. 175, 1749 (1968).

29. K. Schilling et al., Nucl. Phys. B15, 397 (1970), and B18, 332E (1970).

30. N. Schmitz, Proc. of the 1965 Easter School for Physicists, CERN 65-24, Vol.I, June 1965.

31. Y. Eisenberg et al., Phys. Lett. 22, 223 (1966).

32. F. Cooper, Phys. Rev. 167, 1314 (1968).

33. G. Cohen-Tannoudji et al., Nuovo Cim. 55A, 412 (1968).

34. T.M. Knasel, DESY Report No. 70/3 (1970), unpublished.

35. J. Jost et al., Phys. Rev. 80, 189 (1950).

36. K.J. Mork, Phys. Rev. 160, 1065 (1967).

37. K.J. Mork and H. Olsen, Phys. Rev. 140, B1661 (1965).

38. D. Notz, Diplomarbeit Universität, Hamburg (see Ref. 34).

39. T.M. Knasel, Thesis Harward University (1967).

40. G. McClellan et al., Phys. Rev. Lett. 26, 1593 (1971).

41. G. Smadja et al., Phys. Lett. 41B, 635 (1972).

42. S.D. Drell and K. Hiida, Phys. Rev. Lett. 7, 199 (1961); R.T. Deck, ibid 13, (1964).

43. R.T. Poe et al., Phys. Rev. Lett. 22, 551 (1969).

44. F.J. Gilman et al., Phys. Lett. 31B, 387 (1970).

*****